Plasma Membrane Ca^{2+}-ATPase Extrudes Ca^{2+} from Hair Cell Stereocilia

Ebenezer N. Yamoah,[1,3] Ellen A. Lumpkin,[4] Rachel A. Dumont,[1] Peter J. S. Smith,[3] A. J. Hudspeth,[4] and Peter G. Gillespie[1,2]

Departments of [1]Physiology and [2]Neuroscience, The Johns Hopkins University, Baltimore, Maryland 21205, [3]BioCurrents Research Center, Marine Biological Laboratory, Woods Hole, Massachusetts 02543, and [4]Howard Hughes Medical Institute and The Rockefeller University, New York, New York 10021

Mechanically sensitive hair cells of the auditory and vestibular systems use Ca^{2+} to control adaptation of mechanical transduction, to effect frequency tuning, to trigger neurotransmitter release, and to mediate efferent synaptic signaling. To determine the role that pumps play in regulation of Ca^{2+} in the hair bundle, the organelle responsible for mechanoelectrical transduction, we localized and quantified the plasma membrane Ca^{2+}-ATPase (PMCA) of the bundle. We found that each hair bundle contains $\sim 10^6$ PMCA molecules or ~2000 per square micrometer of bundle membrane and that PMCA is the principal calmodulin binding protein of the bundle. Consistent with biochemical estimates of PMCA density, we measured with extracellular Ca^{2+}-selective electrodes a substantial Ca^{2+} efflux from bundles. The number of bundle Ca^{2+} pumps and magnitude of resting Ca^{2+} efflux suggested that PMCA should generate a substantial membrane current as bundles expel Ca^{2+}. Measurement of whole-cell currents revealed a transduction-dependent outward current that was consistent with the activity of PMCA. Finally, dialysis of hair cells with PMCA inhibitors led to a large increase in the concentration of Ca^{2+} in bundles, which suggests that PMCA plays a major role in regulating bundle Ca^{2+} concentration. Our data further indicate that PMCA could elevate the extracellular Ca^{2+} concentration close to hair bundles above the low level found in bulk endolymph.

Key words: hair cell; hearing; calcium; ATPase; stereocilia; hair bundle; ion-selective probe

Hair cells, the receptor cells of the auditory and vestibular systems, transduce mechanical stimuli into changes in membrane potential (for review, see Hudspeth, 1989). A hair cell carries out mechanoelectrical transduction with its hair bundle, a sensory organelle that pivots back and forth in response to sound or head position stimuli. In the sacculus of the American bullfrog, *Rana catesbeiana*, a hair bundle consists of ~60 actin-filled processes called stereocilia and a lone true cilium, the kinocilium (Jacobs and Hudspeth, 1990). Extracellular filaments called tip links interconnect adjacent stereocilia near their tips (Pickles et al., 1984); each link controls one or two active transduction channels (Hudspeth, 1982; Holton and Hudspeth, 1986; Denk et al., 1995; Lumpkin and Hudspeth, 1995). Movement of the bundle in the direction of the kinocilium stretches tip links and opens transduction channels, whereas movement in the opposite direction reduces tip link tension and allows channels to close.

Although transduction channels can pass a broad range of cations (Corey and Hudspeth, 1979; Ohmori, 1985), transduction channels are selective for Ca^{2+} over monovalent cations (Jørgensen and Kroese, 1995; Lumpkin et al., 1997). The Ca^{2+} that enters through transduction channels is critical for hair bundle function. Ca^{2+} regulates adaptation, the process by which hair cells continuously readjust their sensitivity to small displacements (Eatock et al., 1987; Crawford et al., 1991). Ca^{2+} also is required to evoke hair bundle twitches, which may contribute to high-sensitivity displacement detection (Benser et al., 1996). Finally, an elevated Ca^{2+} concentration in stereocilia with active transduction channels may suppress supernumerary tip link formation (Zhao et al., 1996). Control of intracellular Ca^{2+} concentration is therefore critical for stereocilia, which have no intracellular compartments in which to sequester Ca^{2+} and are exposed to an extracellular fluid, endolymph, incompatible with Na^+-dependent Ca^{2+} extrusion.

Recent reports have indicated that cochlear stereocilia contain plasma membrane Ca^{2+} ATPase molecules (PMCA; Crouch and Schulte, 1995) and that PMCA isoforms 1b, 2b, 3a, 3c, and 4b are present in the cochlea (Crouch and Schulte, 1996). In this report we localize PMCA in bullfrog hair cells and estimate that its density is ~2000 pump molecules per square micrometer of stereociliary membrane. Bundle PMCA is active: we measure a substantial, vanadate-sensitive Ca^{2+} efflux from bundles with extracellular Ca^{2+}-sensitive self-referencing electrodes. Analysis of transduction currents reveals an outward current that possesses a pharmacological profile consistent with PMCA activity. Finally, we show that PMCA contributes significantly to control of the hair bundle Ca^{2+} concentration.

Received Aug. 7, 1997; revised Oct. 28, 1997; accepted Oct. 31, 1997.

This work was supported by National Institutes of Health Grants to E.N.Y. (DC03040), P.J.S.S. (RR01395), A.J.H. (DC00241), and P.G.G. (DC00979). A.J.H. is an Investigator and E.A.L. is a Predoctoral Fellow of the Howard Hughes Medical Institute. P.G.G. is a Pew Scholar in the Biomedical Sciences. We thank Drs. W. M. Roberts and F. Jaramillo for advice on diffusion modeling. We also appreciate constructive comments on this manuscript that were provided by Drs. D. Hilgemann and D. Kosk-Kosicka and members of the Hudspeth and Gillespie laboratories. We acknowledge gifts of PMCA from Drs. D. Kosk-Kosicka and G. Inesi.

Correspondence should be addressed to Dr. Peter G. Gillespie, Department of Physiology, The Johns Hopkins University, 725 North Wolfe Street, Baltimore, MD 21205.

Dr. Yamoah's present address: Department of Cell Biology, Neurobiology, and Anatomy, University of Cincinnati, Cincinnati, OH 45267.

 0270-6474/98/180610-•$05.00/0

MATERIALS AND METHODS

Materials. The anti-PMCA monoclonal antibody 5F10 was obtained as undiluted ascites fluid from Affinity BioReagents (Golden, CO). Donkey serum, as well as Cy3-conjugated secondary antibodies, was obtained from Jackson ImmunoResearch Labs (West Grove, PA). Blotting membrane blocking solutions, horseradish peroxidase-coupled secondary antibodies, and chemiluminescence reagents used for immunoblotting (ECL) came from Amersham (Arlington Heights, IL). Streptavidin-alkaline phosphatase and the chemiluminescence reagent used for detection of biotinylated protein [3-(4-methoxyspiro{1,2-dioxetane-3,2′-(5′-chloro)tricyclo[3.3.1.1^{3,7}]decan}-4-yl)phenyl phosphate] (CSPD) were obtained from Tropix (Bedford, MA). Protein G-Sepharose, phenyl-Sepharose, and CNBr-Sepharose were obtained from Pharmacia (Piscataway, NJ). Fluka Chemical (Ronkonkoma, NY) was the source of *N*,*N*-dimethyltrimethylsilylamine and Ca^{2+}-Ionophore I—Cocktail A. Polyvinylidene fluoride (PVDF) membranes (Immobilon P) were purchased from Millipore (Bedford, MA). Fluo-3 (pentapotassium salt) and 5- and 6-carboxyeosin were obtained from Molecular Probes (Eugene, OR). *N*-hydroxysulfosuccinimidobiotin (sulfo-NHS-biotin) was purchased from Pierce (Rockford, IL). Acrylamide, bisacrylamide, ammonium persulfate, *N*,*N*,*N*′,*N*′-tetramethylethylenediamine (TEMED), and SDS were purchased from Bio-Rad (Hercules, CA). Sodium orthovanadate came from Fisher Scientific (Pittsburgh, PA). Sigma (St. Louis, MO) was the source of bovine hemoglobin (H-2500), bovine serum albumin, HEPES, Tris base, Triton X-100, Na_2ATP, and 3-(cyclohexylamino)-1-propanesulfonic acid (CAPS).

Immunocytochemistry. Hair cells were isolated mechanically from the sacculus of *Rana catesbeiana* as described (Assad and Corey, 1992; Yamoah and Gillespie, 1996) in frog saline solution containing (in mM) 110 NaCl, 2 KCl, 3 D-glucose, and 5 HEPES, adjusted to pH 7.3 with NaOH that contained 100 μM $CaCl_2$. Subsequent manipulations used a similar saline solution containing 4 mM $CaCl_2$. Cells were fixed for 20 min with 0.4% formaldehyde, washed, and then permeabilized in 1% Triton X-100 for 10 min. Next they were incubated in a blocking solution (1% bovine serum albumin and 1% donkey serum) for 1 hr, followed by a 2–3 hr incubation with 5F10 monoclonal antibody at a dilution of 1:200 to 1:1000. Hair cells were incubated in secondary antibodies (donkey anti-mouse conjugated with Cy3) for 2 hr, washed, and viewed with a Zeiss LSM 410 confocal microscope. For preadsorption control experiments, the 5F10 antibody was incubated with 5 μg/ml PMCA from rat skeletal muscle before use.

Immunoblotting. Hair bundles and residual macula samples were isolated as previously described (Gillespie and Hudspeth, 1991a). Human erythrocyte PMCA, a gift of Dr. D. Kosk-Kosicka (Department of Anesthesiology, Johns Hopkins University, Baltimore, MD), was purified and quantified as described in Kosk-Kosicka and Inesi (1986). Proteins were separated by SDS-PAGE, using 10% acrylamide gels with a 150:1 acrylamide-to-bisacrylamide ratio, and transferred to PVDF blotting membranes at 100 V for 2 hr with cooling in 5% methanol and 10 mM CAPS, pH 11. To prevent losses of picogram amounts of protein, we included 5 μg of hemoglobin in each sample and added 0.25 mg/ml hemoglobin to the pretransfer incubation solution (Gillespie and Gillespie, 1997). Procedures for SDS-PAGE and electrotransfer have been described in detail elsewhere (Gillespie and Hudspeth, 1991a,b; Gillespie and Gillespie, 1997; Hasson et al., 1997). Membranes were blocked for 2 hr with a proprietary blocking solution (Amersham Liquid Block) diluted to 5% with PBS (150 mM NaCl and 70 mM sodium phosphate, pH 7.4) and then were incubated for 2 hr with a 1:1000 dilution of 5F10 in the blocking solution. After three washes with 0.3% Tween-20 in PBS, blots were incubated for 1 hr with a 1:2500 dilution of horseradish peroxidase-coupled goat anti-mouse antibodies. Blots were washed four to five times with 0.3% Tween in PBS and then once with PBS. Subsequent detection of bound antibodies was completed with enhanced chemiluminescence, using the manufacturer's development methods. All procedures except electrotransfer were performed at room temperature. PMCA in hair bundles was quantified from blots that contained hair cell samples and purified PMCA in known amounts that bracketed the amounts present in hair cell samples. Films were digitized by an eight-bit scanner with a transmission attachment (UMAX UTA-II); NIH Image (version 1.59) was used to calculate the relative intensities of each band. A standard curve was constructed by using the intensities of the purified PMCA standards; the amount of PMCA present in hair cell samples was obtained by interpolation.

Immunoprecipitation. Purified hair bundles were permeabilized and labeled with sulfo-NHS-biotin (Gillespie and Hudspeth, 1991a,b). Detergent-soluble proteins were extracted with 1% Triton X-100 with 0.1 mg/ml bovine serum albumin as a carrier protein. The immunoprecipitation solution also contained 150 mM NaCl, 1 mM dithiothreitol, 10 μM leupeptin, 10 μM pepstatin, 200 μM phenylmethylsulfonyl fluoride, and 25 mM HEPES, pH 7.5. Calmodulin was purified from bovine brain by virtue of its Ca^{2+}-sensitive binding to phenyl-Sepharose (Gopalakrishna and Anderson, 1982); calmodulin-agarose was prepared by coupling purified calmodulin to CNBr-Sepharose according to the manufacturer's instructions. Triton X-100 extracts were incubated in the presence of 0.5 mM $CaCl_2$ with calmodulin-agarose beads for 2 hr at room temperature; beads were washed thoroughly with immunoprecipitation solution containing 0.5 mM Ca^{2+}. Calmodulin binding proteins were eluted with 5 mM EGTA. Triton X-100 extracts or calmodulin-agarose eluates were incubated for 2 hr with 5F10 antibody diluted 1:100 in immunoprecipitation solution; antibodies and bound bundle proteins were separated from the supernatant fluid by adding 5 μl of protein G-Sepharose, incubating for 30 min, and microcentrifuging to sediment the protein G-Sepharose complex. After a thorough washing with immunoprecipitation solution, antibodies and bound bundle proteins were eluted with a SDS-PAGE sample buffer that included 1.5% SDS. Proteins were electrophoresed and transferred to blotting membranes as described above; using methods previously described in detail (Gillespie and Hudspeth, 1991b), we detected biotinylated bundle proteins by using streptavidin-alkaline phosphatase at a dilution of 1:5000 and the chemiluminescence substrate CSPD.

Ca^{2+}-selective self-referencing electrodes. We monitored local Ca^{2+} fluxes near isolated hair cells, using the Ca^{2+}-selective self-referencing electrode technique (Smith et al., 1994). Electrodes were pulled from 1.5 mm diameter borosilicate glass with tip diameters of 1.5–2.5 μm, dried at 180°C overnight (reducing tip size to 1–1.5 μm), and rendered hydrophobic with *N*,*N*-dimethyltrimethylsilylamine (Ammann, 1986). The electrodes were tip-filled with a 15–30 μm column of a Ca^{2+}-ionophore cocktail (10% w/v Ca^{2+}-sensitive neutral carrier ETH 1001, 89% w/v 2-nitrophenyl octyl ether, and 1% w/v sodium tetraphenylborate) and were back-filled with 100 mM $CaCl_2$ in a 0.5% agar gel (Smith et al., 1994; Yamoah and Smith, 1994). Electrodes were calibrated by measuring their static responses to solutions containing 0.1, 1, and 1 mM Ca^{2+} (Kuhtreiber and Jaffe, 1990; Smith et al., 1994); for a 10-fold change in Ca^{2+} concentration, the change in voltage (or sensitivity, *S*) was ~28 mV.

Recordings were performed in frog saline solution with 50 μM $CaCl_2$. The electrode was moved back and forth between two measuring positions, 2.5–10 μm apart. For measurements of Ca^{2+} flux around hair cells, the point of closest approach of the electrode was <1 μm away from a hair bundle or soma. Flux values calculated from the differential voltage measured between these points were compared with background values 300–400 μm away, outside of the calcium gradient induced by cell activity. The frequency of movement (0.3–0.5 Hz) was sufficiently slow to allow the reestablishment of Ca^{2+} gradients before data collection but was adequately fast to minimize the problems inherent in stationary Ca^{2+} electrodes (Smith et al., 1994). The voltages at each measuring position were amplified 1000 times and digitized (DT 2800 series analog-to-digital board; Data Translation, Marlborough, MA). Using DVIS3 software, we collected, pooled, and analyzed data as previously described (Smith et al., 1994). To minimize the impact of noise, particularly slow random drift, we pooled differential voltage values in a running average; the apparent response of the electrode therefore was slowed by the averaging process. To convert voltage readings to a net flux value, we determined the electrode efficiency (R_v) to be 45% (Smith et al., 1994). R_v reflects both the gain of the amplifier and the signal attenuation caused by the response of the ionophore. The liquid exchange membrane used here requires ~10 sec to give a 90% response; the choice of movement frequency for the electrode necessitates an inevitable compromise among allowing reestablishment of a gradient, permitting the ionophore to respond maximally, and minimizing the unavoidable drift. The difference in Ca^{2+} concentration (ΔC) between the extremes of electrode excursion (Δr) was determined from:

$$\Delta C \approx \frac{2.3\ \Delta V\ C_b}{S\ R_v},$$

in which ΔV is the potential difference over the electrode excursion and C_b is the background Ca^{2+} concentration. The flux was determined from this concentration difference and the diffusion coefficient (D):

$$J = -D\ \Delta C\ \Delta r.$$

In some experiments the point of closest approach of the electrode was retracted systematically from the bundle; data from these experiments were fit via the following equation (Smith et al., 1994):

$$\Delta V = \frac{-S\,R_v\,K\,\Delta r}{2.3(C_b r^2 + Kr)},$$

in which r is the distance from the source of Ca^{2+} to the electrode at its measurement position and K is an empirical constant. Amplifiers, headstages, motion control systems, and software were all produced at the BioCurrents Research Center of the Marine Biological Laboratory (Woods Hole, MA).

Stock solutions of 200 mM sodium orthovanadate were made at pH 10, boiled to eliminate polymeric species (Goodno, 1982), and stored at −20°C. Mechanical stimulation of the hair bundle was conducted with a two-dimensional piezoelectric bimorph stimulator (Corey and Hudspeth, 1980). For microinjection, pipettes were pulled from 1.5 mm borosilicate glass; their tip resistances were 40–50 MΩ. Pipettes were filled with (in mM) 85 KCl, 3 $MgCl_2$, 2 Na_2ATP, 1 EGTA, and 5 HEPES, with or without 0.2 mM vanadate. Microinjection was performed with a Narashigi IM-200 pressure controller (Narashigi USA, Sea Cliff, NY). The optimal injection pressure was determined by injection of Lucifer yellow in 1 M LiCl; five 2 sec pulses within 1 min, in continuous mode at 3 kPa, gave efficient loading without cell disruption. Injection of control and vanadate solutions used identical settings.

Whole-cell recording. An Axopatch 200A amplifier (Axon Instruments, Foster City, CA) was used to record transduction currents from isolated cells at a holding potential of −80 mV with the tight-seal, whole-cell voltage-clamp technique. Bundle displacement used the stimulator described above; the kinociliary bulb of the bundle was held tightly with modest suction through a glass micropipette that served as a stimulus probe. This configuration prevented slippage of the bundle relative to the stimulus probe, a degree of stability essential for interpretation of small membrane currents. In most cases, mechanical stimuli had durations of 100–1000 msec with an interstimulus interval of 1.5 sec; alternating positive and negative displacements were provided. The recording electrode solution contained (in mM) 85 CsCl, 3 $MgCl_2$, 2 Na_2ATP, 1 EGTA, and 5 HEPES. CsOH was used to adjust the final pH to 7.3. Frog saline solution containing 4 mM $CaCl_2$ and oxygenated at room temperature was used as the bath solution. Other recording conditions were similar to those described earlier (Yamoah and Gillespie, 1996).

Detection of stereociliary Ca^{2+}. Hair cells were isolated as described previously (Lumpkin and Hudspeth, 1995) and were bathed in frog saline solution containing 4 mM Ca^{2+}. We clamped membrane potentials at −70 mV with tight-seal whole-cell electrodes, using a voltage-clamp amplifier (EPC-7, List Electronics, Darmstadt, Germany). The electrodes contained (in mM) 100 CsCl, 2 Na_2ATP, 3 $MgCl_2$, 0.5 fluo-3 (pentapotassium salt), and 5 HEPES; the pH was adjusted to 7.26 by the addition of 6 mM CsOH. When noted, 1 mM vanadate or 5 μM carboxyeosin was added to the internal solution. Transduction was verified by measurement of transduction currents or, in one control cell, by the presence of elevated fluorescence at stereociliary tips (a tip blush; Lumpkin and Hudspeth, 1995). To elicit a transduction current, we displaced a hair bundle 300 nm in the positive direction with a glass micropipette. Maximal transduction currents for cells dialyzed with vanadate ranged from −40 to −190 pA, those for cells dialyzed with carboxyeosin ranged from −40 to −215 pA, and those for control cells ranged from −70 to −190 pA. Because the fluorescence signals became variable as cells became leaky, data collected after the leakage current of a cell exceeded −250 pA were excluded from the study.

To detect changes in the free Ca^{2+} concentration of hair bundles, we simultaneously visualized hair cells loaded with fluo-3 via epifluorescence and differential interference contrast optics with a Zeiss LSM 410 confocal microscope equipped with a 63×, oil-immersion objective lens of numerical aperture 1.4. The line scan mode of the confocal microscope was used to follow fluorescence changes in a hair bundle at 1.4 msec intervals before, during, and after positive displacements. To minimize variability between cells, we imaged the focal plane in each cell in which the fluorescence intensity of the bundle was maximal. To ensure that fluorescence intensities could be compared between cells, we normalized raw intensity data by the confocal gain; other settings were held constant during image acquisition. All images were processed identically with NIH Image 1.59.

To estimate the fluorescence intensity of the hair bundle in each image, we used a graphics cursor provided by the software of the confocal system (LSM 3.95, Zeiss, Jena, Germany) to outline a region encompassing only the hair bundle. The intensities of pixels within the specified area then were averaged. To determine the somatic fluorescence, we similarly measured the average intensity of a region just below the cuticular plate and above the nucleus. In healthy cells the fluorescence of this somatic region was homogeneous.

An estimate of the resting free Ca^{2+} concentration in these hair bundles was obtained according to Kao et al. (1989). Because the fluorescence of fluo-3 with Ca^{2+} bound exceeds that of fluo-3 without Ca^{2+} by at least 40-fold, the fluorescence contribution of free fluo-3 was ignored in the calculation. The dissociation constant of the indicator for Ca^{2+} was set at 400 nM (Eberhard and Erne, 1989). To determine the value for maximal fluo-3 fluorescence, we measured the fluorescence of control internal solution supplemented with 11 mM $CaCl_2$ with the same confocal settings as those used in the hair bundle Ca^{2+} imaging experiments.

In these experiments the fluorescence increase observed during each whole-cell recording represented both the rate of fluo-3 diffusion into the hair bundle and the rate of Ca^{2+} accumulation in the cell. In healthy control cells the resting free Ca^{2+} concentration should have been quite stable over minutes; such stability was confirmed in cells loaded with the membrane-permeant acetoxymethyl ester of fluo-3 and then voltage-clamped in the perforated patch configuration (data not shown). Because little Ca^{2+} initially accumulated in control cells, the fluorescence increase in these cells at early time points probably reflected the rate of fluo-3 diffusion from the whole-cell recording pipette into hair bundles. As a result, our calculations of the free Ca^{2+} concentration that used the *in vitro* calibration of maximal fluo-3 fluorescence, especially those at early time points, are likely to be underestimates. Comparisons between cells at similar time points nonetheless are valid.

RESULTS

Localization of PMCA in bullfrog hair cells

To examine the distribution of PMCA in bullfrog saccular hair cells, we used confocal immunofluorescence microscopy with a monoclonal antibody that binds all known PMCA isoforms in many species (5F10; Adamo et al., 1992). We saw consistent labeling of hair cells (Fig. 1*A,B*), which was abolished when the antibody was preincubated with purified PMCA (Fig. 1*C*). Hair bundles were intensely labeled. In hair cells with broad bundles, labeling was concentrated somewhat at stereociliary tips but otherwise was distributed relatively uniformly along the stereocilia (Fig. 1*A*). By contrast, in hair cells with narrow bundles, labeling frequently was observed in a broad band starting above the basal tapers, where stereocilia narrow before somatic insertion, as well as at stereociliary tips (Fig. 1*B*). In both types of hair bundles, labeling appeared relatively weak both in the taper region and in the basal connector region, a narrow zone characterized in frog hair cells by cross-links between stereocilia (Jacobs and Hudspeth, 1990). Although labeling of the basolateral membrane of the cell appeared faint in comparison to that of the hair bundle, the large amount of membrane in optical sections of hair bundles probably contributed to the apparent discordance in labeling intensity. Labeling appeared uniform along the basolateral membrane, with no evidence for discrete densities of pumps near the aggregates of Ca^{2+} channels found at neurotransmitter release sites (Roberts et al., 1990; Issa and Hudspeth, 1994).

Estimation of bundle PMCA by quantitative immunoblotting

We used quantitative immunoblotting to estimate the amount of PMCA in hair bundles. We purified hair bundles with the twist-off technique (Gillespie and Hudspeth, 1991a), subjected bundle proteins to SDS-PAGE, transferred the proteins to a blotting membrane, and detected PMCA with the 5F10 antibody. This antibody detected bands at molecular masses 140 and 170 kDa in purified bundles and in the residual macula, the supporting and

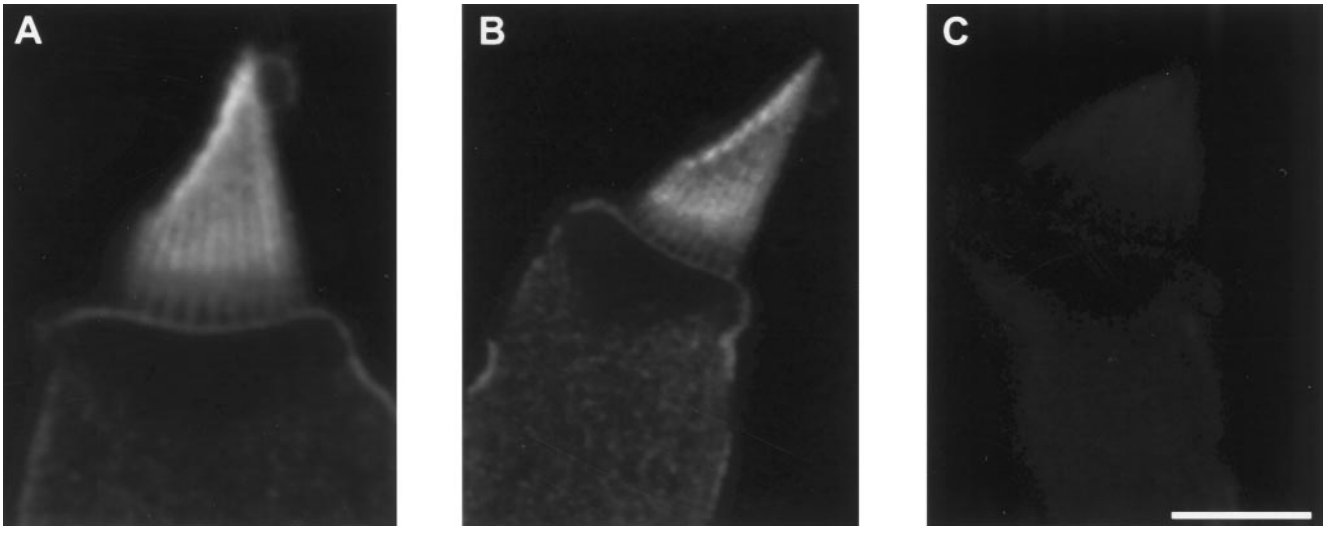

Figure 1. Immunocytochemical localization of PMCA in isolated hair cells. *A, B,* Plasma membranes of hair cells were labeled by the 5F10 anti-PMCA monoclonal antibody. Hair bundles appeared more intensely labeled than basolateral membranes, in part because the concentration of plasma membrane in optical sections through hair bundles exceeds that in views of the basolateral membrane. The labeling of broad hair bundles (*A*) was usually more uniform than that of narrow hair bundles (*B*). Labeling was often strongest at stereociliary tips. The basal connector region, immediately above the stereociliary tapers, was labeled relatively weakly. *C,* Labeling was blocked when immunocytochemistry was performed in the presence of 5 μg/ml purified red blood cell PMCA. The 5 μm scale bar applies to all three panels.

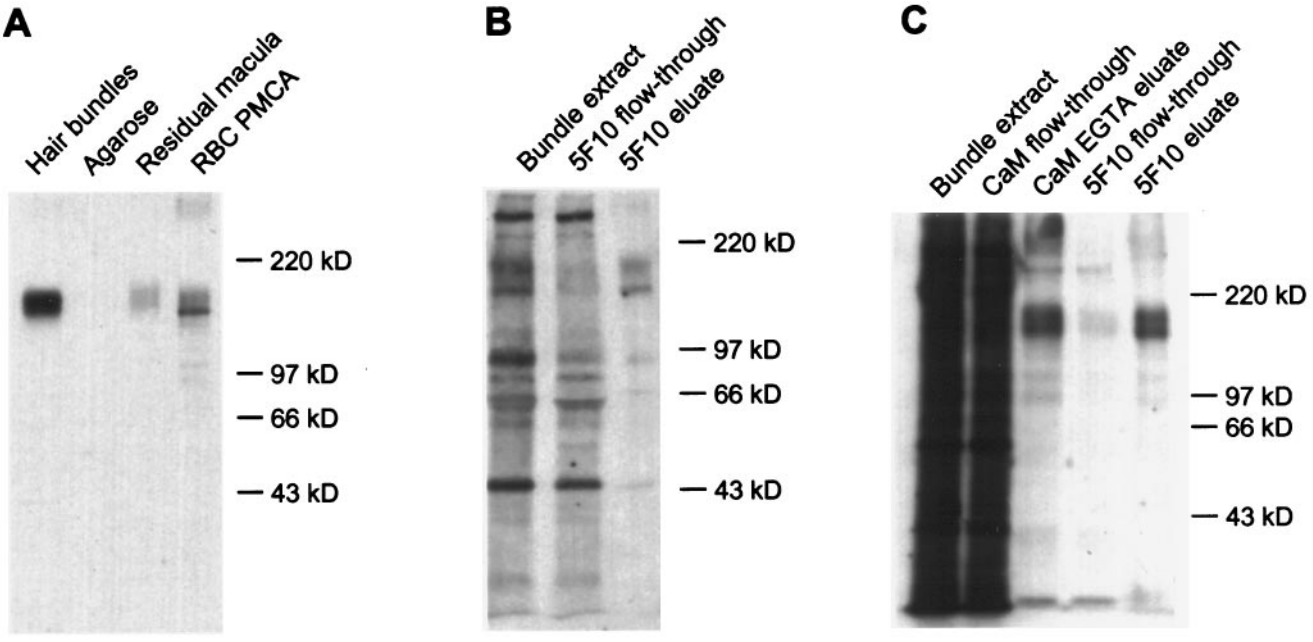

Figure 2. Detection of hair bundle PMCA with the 5F10 antibody. *A,* Immunoblot detection of proteins of 140 and 170 kDa in isolated hair bundles and residual macula, the sensory epithelium remaining after hair bundle isolation, with anti-PMCA monoclonal antibody (5F10). *Hair bundles*, From 21 frog sacculi (~42,000 bundles in agarose gel); *Agarose*, equivalent amount of agarose gel; *Residual macula*, 0.5 saccular equivalents; *RBC PMCA*, purified human erythrocyte PMCA (5000 pg). *B,* Immunoprecipitation of PMCA with 5F10 from a Triton X-100 extract of purified, biotinylated hair bundles. Equal fractions of the Triton X-100 bundle extract, flow-through solution from the 5F10 anti-PMCA antibody precipitation, and 5F10 SDS eluate were loaded. *C,* Immunoprecipitation of 140 and 170 kDa calmodulin binding proteins with 5F10 from purified, biotinylated hair bundles. Calmodulin binding proteins were isolated first from a Triton X-100 extract of purified, biotinylated hair bundles, using calmodulin-agarose; then the EGTA eluate from the calmodulin-agarose was used for precipitation of PMCA with 5F10. Equal fractions of each sample were loaded.

hair cell epithelium remaining after bundle isolation (Fig. 2*A*; the separation between the two bands is seen better with lighter exposures). Although 140 kDa corresponds to the molecular mass of several PMCA isozymes (Carafoli, 1991), PMCA molecules with primary sequences encoding 170 kDa molecules have not been reported previously. Neither form shifted in migration after treatment with *N*-glycanase F (data not shown), suggesting that the larger species did not arise from glycosylation of the 140 kDa form. Because purified PMCA can form a higher mass band under certain sample preparation conditions (D. Kosk-Kosicka, personal communication), the 170 kDa band might have derived artifactually from the 140 kDa form. Considering the 140 and 170

kDa bands together, using purified PMCA from human erythrocytes as a standard, and assuming that the frog bundle PMCA has identical immunoreactivity, we estimated that the bundles from one sacculus contain 330 ± 100 pg of PMCA (mean ± SD, $n = 4$). Assuming that a typical sacculus has ~2000 hair bundles (Benser et al., 1993) and that each of the ~60 stereocilia has an average plasma membrane surface area of 8.5 μm^2 (Jacobs and Hudspeth, 1990), the average PMCA density is ~1300 μm^{-2}.

Quantitation of bundle PMCA by calmodulin receptor content

The similarity in size of the bands reactive with the 5F10 antibody to the major calmodulin binding proteins of the hair bundle (Walker et al., 1993) indicated that we could derive an independent estimate of the density of hair bundle PMCA from the known concentration of calmodulin receptors. To identify PMCA, we used the 5F10 antibody to immunoprecipitate proteins from Triton X-100 extracts of biotinylated hair bundles. Two proteins were immunoprecipitated (Fig. 2*B*) that were similar in mass to the proteins seen by immunoblotting. To confirm that these proteins are the major calmodulin binding proteins, we conducted successive precipitations with calmodulin-agarose and 5F10. Several bundle proteins bound to calmodulin-agarose and were eluted with EGTA; the protein pattern corresponded remarkably well to that obtained by using calmodulin-alkaline phosphatase to probe blots of bundle proteins (Walker et al., 1993; Walker and Hudspeth, 1996). Of the proteins eluted from calmodulin-agarose, only the 140 and 170 kDa proteins subsequently were precipitated with 5F10 (Fig. 2*C*). In combination with immunoblotting and calmodulin-alkaline phosphatase overlay results, these results indicate that hair bundles contain two species of PMCA of molecular masses 140 and 170 kDa, both of which bind calmodulin.

Of the 12.5 fmol of calmodulin in each saccular equivalent of hair bundles (Walker et al., 1993), ~45% is bound in a Ca^{2+}-dependent manner to Triton X-100-soluble receptors (Walker et al., 1993) (data not shown). Furthermore, of the detergent-soluble calmodulin receptors, PMCA accounts for ~85% of the binding sites. If we assume that one molecule of calmodulin binds to each PMCA molecule (Hinds and Andreasen, 1981), these data indicate that the hair bundles derived from one sacculus contain 4.8 fmol of PMCA. This value corresponds to a density of ~2800 μm^{-2} on stereociliary membranes. Given the uncertainties associated with each method, this estimate corresponds well with that obtained by protein immunoblotting.

Local Ca^{2+} efflux from hair cells

Because our biochemical data suggested that substantial amounts of PMCA exist on hair bundle membranes, we reasoned that the local Ca^{2+} efflux from bundles could be substantial. Using Ca^{2+}-selective self-referencing electrodes (Smith et al., 1994), which detect local Ca^{2+} gradients with a resolution of a few micrometers, we examined the local Ca^{2+} flux at different regions of hair cells in a bath solution containing 50 μM Ca^{2+}. The efflux of Ca^{2+} from the base of a resting hair bundle exceeded that from the basolateral membrane of the cell (Fig. 3*A*). Retraction of the electrode from the bundle indicated that Ca^{2+} flux diminished with distance; the data were fit approximately with a model that assumes a point source within the bundle (Fig. 3*B*; Smith et al., 1994). The fit would have been qualitatively similar if the model instead had incorporated a set of point sources distributed within the bundle, viewed from the outside. The local Ca^{2+} flux immediately adjacent to hair bundles (-5 ± 2 nmol m^{-2} sec^{-1}; $n = 9$) significantly ($p < 0.005$; one-tailed Student's t test) exceeded that measured near basolateral membranes (-2 ± 1 nmol m^{-2} sec^{-1}; $n = 9$) or in background regions (0 ± 1 nmol m^{-2} sec^{-1}; $n = 9$).

By careful placement of the electrode near the top of a hair bundle, we could measure either local Ca^{2+} efflux or influx, depending on mechanical stimulation. When a hair bundle was first displaced in the negative direction, closing most transduction channels, an electrode positioned next to the top of the bundle measured a local Ca^{2+} efflux; then when the bundle was moved in the positive direction, opening transduction channels, the signal reversed and a local Ca^{2+} influx was measured (Fig. 3*C*).

Although not selective for PMCA (Macara, 1990), vanadate potently inhibits this Ca^{2+} pump (Carafoli, 1991). Ca^{2+} efflux from resting hair bundles was reduced on the microinjection into hair cells of internal solution containing 0.2 mM vanadate (Fig. 3*D*) but was unaffected by injection of internal solution alone (data not shown).

Transduction-dependent outward current

Ca^{2+} carries approximately a quarter of the transduction current in cells bathed with frog saline solution containing 4 mM Ca^{2+} (Lumpkin et al., 1997). If the PMCA in hair bundles is electrogenic (Läuger, 1991; Hao et al., 1994) and has a turnover rate similar to that of PMCA in erythrocytes (Garrahan, 1986; Rega, 1986), activation of a significant fraction of the PMCA molecules of the bundle could generate an outward current of several picoamperes as the Ca^{2+} entering during transduction is extruded. We therefore predicted that, under optimal recording conditions, it should be possible to resolve a PMCA current after activation of transduction channels. We next sought to detect and characterize this signal.

To unmask the current component associated with PMCA activity, our experimental protocol involved steps that fixed or eliminated two well characterized components of the membrane current measured from a hair cell with a whole-cell tight-seal recording electrode. First, the ions trickling through the seal between the electrode and plasmalemma produce a leakage current. For negative holding potentials, this component is directed inwardly and hence is negative in sign. By clamping the membrane potential at a constant level, we ensured that the leakage current did not vary during mechanical stimulation but simply added a constant offset to each of our recordings. The flux of cations through mechanoelectrical transduction channels produces a second component of inward membrane current. Because transduction channels generally display a significant open probability in the absence of stimulation, the current entering an undisturbed hair cell includes some transduction current. If the hair bundle is moved sufficiently far in the positive direction, this current grows until all of the channels have opened. Moving the bundle well in the negative direction closes all of the transduction channels, affording us a means of eliminating the transduction current. In each case, to confirm that we could close transduction channels completely, we applied at least two large negative displacements.

The PMCA-associated current usually was measured with a two-step stimulus protocol. We wanted to allow Ca^{2+} entry into stereocilia, so a positive hair bundle deflection was given to elicit a large transduction current. At the conclusion of this prepulse stimulus, the bundle was displaced with a saturating negative test pulse that closed all of the mechanically sensitive channels and thus eliminated the transduction current. Immediately after the onset of the test pulse, this procedure often yielded a small,

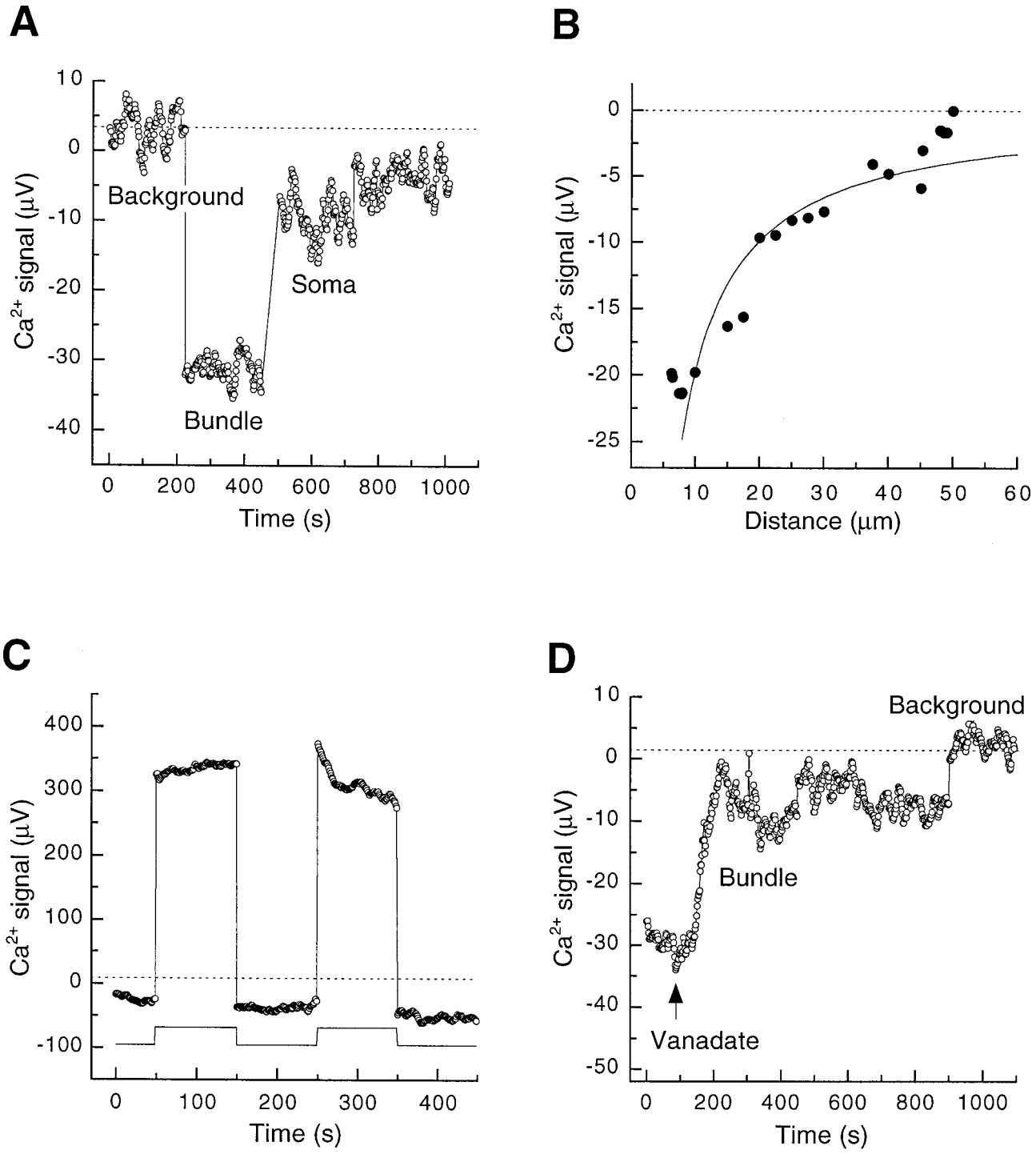

Figure 3. Steady-state Ca^{2+} efflux from hair bundles and basolateral surfaces of isolated hair cells measured with a Ca^{2+}-selective self-referencing electrode. The average background signals are indicated by *dotted lines*. *A,* Ca^{2+} efflux from hair bundles exceeded that from the basolateral membrane. By convention, Ca^{2+} efflux is illustrated as a negative voltage and Ca^{2+} influx as a positive voltage. During the course of the experiment the electrode was moved from a background region to the base of a hair bundle and then to the soma of that cell. *B,* Reduction of Ca^{2+} flux during electrode withdrawal from a hair cell. The measurement position of the electrode was moved to the indicated distances from a hair bundle; a gradient was detectable up to 50 μm away. The *solid line* represents the theoretical gradient calculated as described in the text. *C*, Ca^{2+} influx during transduction. While the extracellular Ca^{2+} flux was measured near the top of the hair bundle, the bundle was deflected in the negative direction (start of record). Positive bundle displacements (indicated *below* the electrode signal) produced a net influx. *D,* Microinjection of vanadate into a hair cell reduced the steady-state Ca^{2+} efflux from the hair bundle. The *arrow* indicates the time at which vanadate was injected. At the end of the experiment the electrode was withdrawn from the bundle to measure the background signal.

transient, positive component of membrane current, which we term the transduction-dependent outward current, or I_{TOC} (*arrows* in Fig. 4*A,B*). We measured I_{TOC} by comparing the difference in membrane current elicited by test pulses after negative and positive prepulses.

Figure 4*A* illustrates a response in which negative displacements established that the leakage current measured −152 pA. When positive prepulse displacements were applied to allow Ca^{2+} entry, however, subsequent negative test pulses induced a membrane current overshoot to approximately −148 pA, or 4 pA further in the outward direction. We attributed this contribution of +4 pA to I_{TOC}. Another cell exhibited a substantial resting open probability, which presumably arose from an unintended positive offset that occurred when the stimulator was attached to the bundle. In this cell the response to the test pulse also differed, depending on whether the prepulse was positive or negative (Fig. 4*B*). A substantial I_{TOC} appeared to flow at rest in this cell and could be suppressed by negative prepulses (Fig. 4*B*). Suppression of I_{TOC} by negative displacements resembled the recovery of current toward the resting level that occurs as a result of adaptation. In Figure 4*B*, however, the increase in inward current during large negative displacements could not have arisen entirely from adaptation; after the termination of the test pulse, the current overshot (to current level *4* in Fig. 4*B*) to a value more negative than that seen during saturating positive prepulse displacements (current level *3*). Current level *4* represents the leak plus fully activated transduction channels; current level *3* represents the leak plus fully activated transduction channels *and* I_{TOC}.

The magnitude of I_{TOC} depended on the prepulse duration: the current grew approximately linearly and reached a maximal value at 300–350 msec (Fig. 4*C*). Decay of the outward current was prolonged also. Although we did not examine the decay of I_{TOC} directly, we noted that the recovery of membrane currents to the resting level after positive displacements of 150 msec duration could be fit by two time constants (29 ± 9 and 136 ± 47 msec; n = 9). The shorter time constant likely reflected adaptation (Eatock et al., 1987), whereas the second component may have corresponded to the decay of I_{TOC}.

We also observed I_{TOC} by allowing the adaptation occurring during a positive stimulus to reduce transduction channel open probability to near zero when the hair bundle was returned to its rest position (Fig. 4*D*). With this stimulus protocol, commonly used for other studies of hair cell transduction (Yamoah and Gillespie, 1996), a saturating negative displacement established the membrane leakage current; any additional outward current after a saturating positive displacement derived from I_{TOC}. Using this definition, we saw I_{TOC} in 21 of 66 recordings in which initial seal resistances were 5 GΩ or larger. When present, I_{TOC} could be as large as 10 pA; for 150 msec displacements I_{TOC} averaged 3.1 ± 1.9 pA (mean ± SD, n = 21). In these 21 cells the maximal transduction currents were −83 ± 26 pA; I_{TOC} thus averaged 0.04 pA per picoampere of inward transduction current.

The PMCA inhibitor vanadate blocked I_{TOC}. After establishing the whole-cell configuration with an electrode containing vanadate, we occasionally observed I_{TOC} (*arrow* in Fig. 5*A*); as vanadate continued to diffuse into the cell, however, I_{TOC} disappeared (Fig. 5*B*). By contrast, when we observed I_{TOC} in cells filled with control solutions, the current often persisted for several minutes. Although vanadate shifted the resting open probability of the transduction channels, presumably by inhibiting adaptation motor myosin molecules (Yamoah and Gillespie, 1996), such a shift cannot explain the results of Figure 5, *A* and *B*. Because negative displacements of increasing amplitudes suppressed transduction to a single current level, these displacements were saturating and hence closed all channels. Nevertheless, the membrane current level after positive displacements in Figure 5*A*—but not Figure 5*B*—moved closer to zero, indicating that additional outward current (I_{TOC}) had been elicited. Despite substantial adaptation in Figure 5*B*, which permitted complete channel closure at the ends of positive steps, the membrane current level did not become more positive than the level associated with complete channel closure. Vanadate must have blocked I_{TOC} rapidly. Similar inhibition of I_{TOC} was seen with BeF_x, but not with SO_4^{2-} (Yamoah and Gillespie, 1996) (data not shown). Although BeF_x probably inhibits PMCA (Murphy and Coll, 1993), SO_4^{2-} does not affect this Ca^{2+} pump (Hao et al., 1994). Because vanadate also inhibits other membrane transporters, we dialyzed hair cells with carboxyeosin, a relatively selective inhibitor of PMCA (Gatto and Milanick, 1993). I_{TOC} disappeared during this treatment in several cells, although sufficient time elapsed in each case that we could not determine whether this inhibition was significant.

I_{TOC} is Ca^{2+}-dependent: reduction of Ca^{2+} entry into stereocilia by replacement of most bath Ca^{2+} with Sr^{2+} reduced I_{TOC} nearly to zero (Fig. 5*C*). Although Sr^{2+} is a substrate for PMCA, its affinity for the pump is at least 10-fold lower than that of Ca^{2+} (Graf et al., 1982).

I_{TOC} did not arise from Ca^{2+}-dependent K^+-channel activity. To minimize any possible contribution by large conductance Ca^{2+}-dependent K^+ (BK) channels, we dialyzed hair cells with Cs^+, which blocks most K^+ channels. To ensure that Cs^+-permeant small conductance Ca^{2+}-dependent K^+ (SK) channels were not the source of I_{TOC}, we demonstrated that I_{TOC} remained even after bath application of 100–500 nM apamin, an inhibitor of SK channels (Fig. 5*D*). Furthermore, any SK current should have been small, given our holding potential and ionic compositions.

Other possible membrane conductances do not contribute to I_{TOC}. Na^+ or Cl^- currents would be inward under our recording conditions; a contribution to I_{TOC} from somatic Na^+/Ca^{2+} exchangers is implausible, both because I_{TOC} was independent of changes in the bath Na^+ concentration (data not shown) and because a Na^+/Ca^{2+} exchanger current should have been inward at −80 mV if the exchanger uses a stoichiometry of 3:1 Na^+/Ca^{2+} or 4:1:1 $Na^+/K^+/Ca^{2+}$ (Reeves, 1991). The Na^+/K^+-ATPase, which occurs at a high density in the basolateral membrane of the hair cell (Burnham and Sterling, 1984), would have produced an outward current. Although substantial amounts of Na^+ enter during transduction, a Na^+/K^+-ATPase current should not have depended on Ca^{2+} entry, and Na^+ pumps should, in any event, have operated at their maximal rate with the saturating concentrations of internal Na^+ and external K^+ that we used (Läuger, 1991). The I_{TOC} data are thus most consistent with PMCA pump activity.

Contribution of PMCA to maintenance of low stereociliary Ca^{2+} concentration

To examine directly the role played by PMCA in hair bundle Ca^{2+} regulation, we monitored the intracellular Ca^{2+} concentration with the indicator fluo-3 while dialyzing hair cells with inhibitors of PMCA. In all cases the inhibitors induced substantial increases in hair bundle Ca^{2+} concentration. The fluo-3 fluorescence intensity, and thus the free Ca^{2+} concentration, was higher in a hair cell dialyzed with 1 mM vanadate (Fig. 6*C,D*) than in a cell filled with control internal solution (Fig. 6*A,B*). Furthermore,

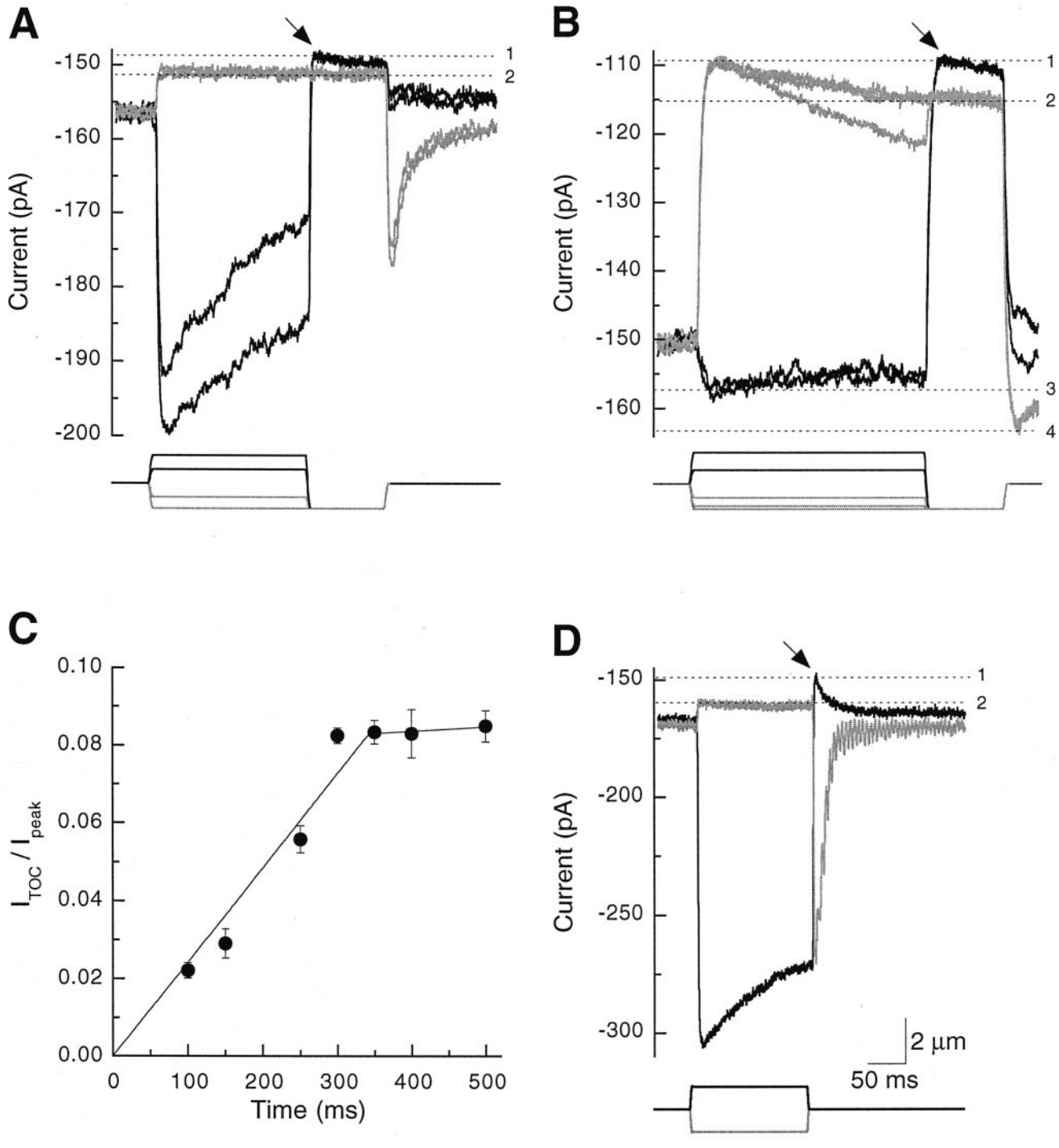

Figure 4. Transduction-dependent outward current. *A, B,* From rest, hair bundles were displaced with prepulses of −1200 to +1500 nm and then were subjected to a −1200 nm test pulse that closed all transduction channels. Mechanical stimuli are indicated at the *bottom* of each panel. *A,* For a cell with a low resting open probability, test pulses after positive prepulse displacements (*black lines*) elicited I_{TOC} (*arrow*); I_{TOC} did not appear after negative prepulses (*gray lines*). The membrane current at level *1* included leakage and I_{TOC} components; that at level *2* was exclusively leakage current. The prepulse stimuli were −1200, −660, +660, and +1320 nm. *B*, For a cell with a high resting open probability, I_{TOC} (*arrow*) was seen after positive displacements (*black lines*) and appeared to be particularly large at rest. Current components at levels *1* and *2* were interpreted as for *A*. The current at level *3* included leakage and I_{TOC} components as well as the maximal transduction current; that at level *4* included only leakage and maximal transduction current components. The prepulse stimuli were −1200, −1060, −660, +660, and +1500 nm. *C*, I_{TOC} increased in amplitude with prolonged displacement. Hair bundles were displaced for increasing durations, using the stimulus protocol described for *A* and *B*. I_{TOC} divided by the peak transduction current (I_{peak}) is plotted against prepulse duration; mean ± SD from three to five cells is plotted. The 0–350 msec and 350–500 msec points were fit separately with least-squares linear regressions. *D,* I_{TOC} appeared after a positive displacement (*black line*) with sufficient adaptation during the step to permit complete transduction channel closure at the termination of the step. The relaxation of current past level *2* after the positive step resulted from adaptation-dependent reopening of transduction channels and slow cessation of I_{TOC}. Current components at levels *1* and *2* were interpreted as for *A*; a smaller negative displacement also produced a current at level *2* (data not shown), indicating that the displayed trace represented the membrane current level at which all channels were closed. The displacements were ± 1080 nm. Scale bars apply to *A*, *B*, and *D*.

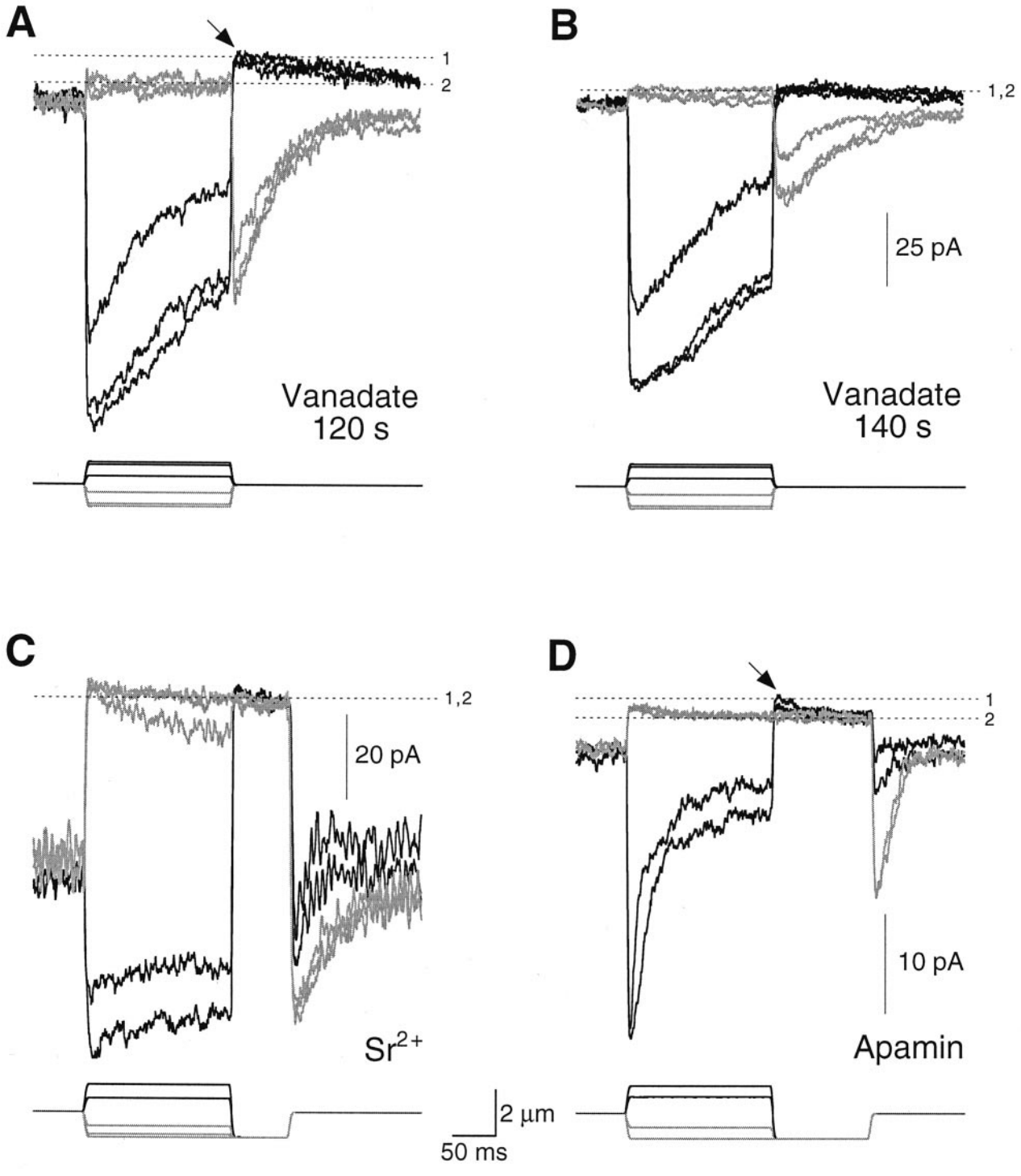

Figure 5. Pharmacological manipulation of the transduction-dependent outward current. Transduction currents arising from positive displacements (*black lines*) and negative displacements (*gray lines*) are plotted; when visible, I_{TOC} is indicated by an *arrow*. The current components at levels *1* and *2* were interpreted as in Figure 4. *A, B,* Vanadate blocked I_{TOC}. After 120 sec of dialysis without mechanical stimulation and with a recording electrode that contained 0.5 mM vanadate, stimulus families were initiated immediately (*A*) or 20 sec later (*B*). I_{TOC} was usually absent after 120 sec of dialysis; in the few cases in which it occurred (e.g., *A*), it was blocked very rapidly. The displacements were −1050, −920, −400, +400, +920, and +1050 nm. *C*, I_{TOC} was present 120 sec after break-in (data not shown) but nearly disappeared within 20 sec of exposure to 2.5 mM $SrCl_2$ and 0.5 mM $CaCl_2$. Although a small I_{TOC} remained in this cell, I_{TOC} was usually not visible with this ionic combination. The prepulse stimuli were −1200, −1050, −660, +660, and +1320 nm; the test pulse was −1200 nm. *D*, I_{TOC} (*arrow*) remained even during the exposure of hair cells to 100 nM apamin, an SK channel blocker (~180 sec after break-in). The prepulse stimuli were −1200, −660, +660, and +1320 nm; the test pulse was −1200 nm. Scale bars between *C* and *D* apply to all panels.

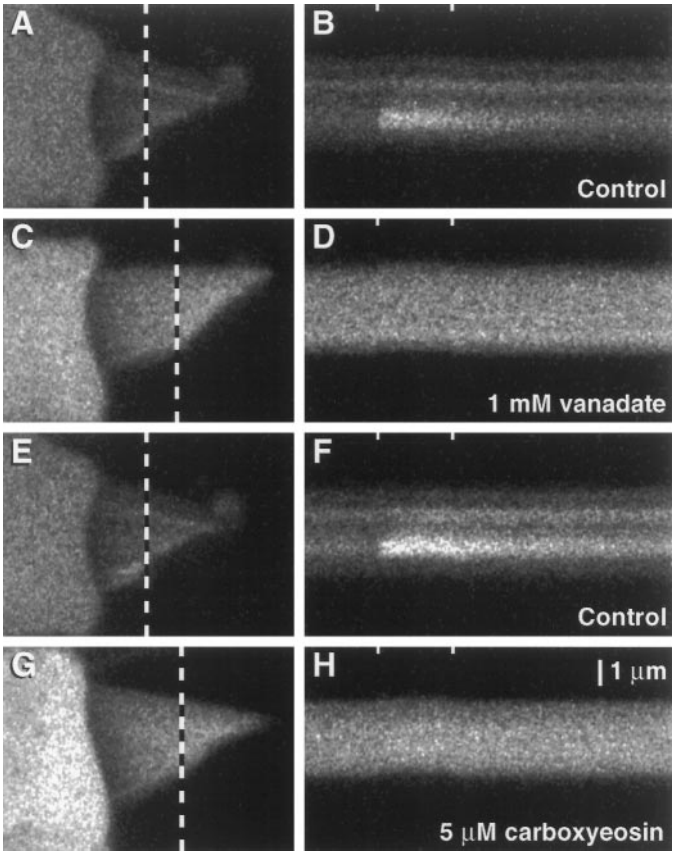

Figure 6. Elevation of the resting free Ca^{2+} concentration in hair cells dialyzed with PMCA inhibitors. Hair cells were dialyzed with fluo-3 and inhibitors of PMCA; fluorescence intensity was measured with confocal microscopy. *A*, *C*, *E*, *G*, Frame scan images acquired before elicitation of transduction currents. The *dotted lines* overlying the hair bundles mark the transects illuminated during the acquisition of the line scan images on the *right*. *B*, *D*, *F*, *H*, Line scan images showing responses to mechanical stimuli; the *tick marks* at the *top* of each panel mark the beginning and end of the 100 msec positive hair bundle deflection. The ordinate represents distance across a hair bundle from the longest stereocilium (*top*) to the shortest (*bottom*); time progresses along the abscissa. *A*, *B*, Control cell, 240 sec after break-in. In *A*, the increased fluorescence intensity observed near the tips of some stereocilia indicated active transduction channels. In *B*, a positive displacement that elicited a −150 pA receptor current also produced elevated fluo-3 fluorescence. The decay of the fluorescence signal after the bundle was returned to rest was declined exponentially with a time constant of 150 msec. *C*, *D*, Cell dialyzed with 1 mM vanadate, 219 sec after break-in. The resting fluorescence was much higher than in the control, and no modulation of the signal was seen despite a transduction current of −165 pA. *E*, *F*, Control cell, 307 sec after break-in. The transduction current was −140 pA; the fluorescence decay after stimulation ended declined exponentially with a time constant of 160 msec. *G*, *H*, Cell dialyzed with 5 μM carboxyeosin, 312 sec after break-in. The resting fluorescence was elevated when compared with that of the control. Despite a transduction current of −175 pA, no modulation of the fluorescence signal was seen. The increased fluorescence signal in the cuticular plate, when compared with that in the hair bundle and soma, apparently was attributable to fluo-3 binding; this phenomenon was observed after several minutes of recording in most hair cells. The scale bar in *H* applies to all panels.

the increase in resting Ca^{2+} concentration precluded the detection of changes in stereociliary Ca^{2+} concentration during mechanoelectrical transduction, despite transduction currents that approached −200 pA. Like vanadate, 5 μM carboxyeosin induced a substantial rise in resting fluo-3 fluorescence (Fig. 6*G,H*) over the level in control cells (Fig. 6*E,F*). The pronounced effects of carboxyeosin in these experiments, compared with the modest effects of the inhibitor in the I_{TOC} experiments, presumably arose because we measured its cumulative effects on Ca^{2+} concentration over the entire recording period. The fluorescence of this low concentration of carboxyeosin was <7% that of the fluo-3 internal solution and thus contributed minimally to the observed fluorescence signal. Similar effects on fluo-3 fluorescence were observed in cells dialyzed with an ADP analog, adenosine 5′-*O*-(2-thiodiphosphate) (ADPβS; data not shown). Although its effects on PMCA have not been tested, we expect that ADPβS also inhibits this Ca^{2+} pump, for it inhibits the intracellular sarcoplasmic/endoplasmic reticulum Ca^{2+}-ATPase (SERCA; Myung and Jencks, 1994). By inhibiting the adaptation motor, ADPβS shifts the resting open probability of the transduction channels from ~0.1 to 0.8 (Gillespie and Hudspeth, 1993), which could lead to enhanced Ca^{2+} influx at rest. To ensure that the observed increase in hair bundle fluorescence did not result from adaptation motor inhibition, we offset each bundle >0.5 μm in the negative direction immediately after establishing the whole-cell configuration so that transduction channels were predominately closed when the bundle was unstimulated.

The absolute intensity of fluo-3 fluorescence in the hair bundles of cells filled with vanadate and carboxyeosin exceeded those of control cells. In addition, the rate of fluorescence increase over the first 400 sec of whole-cell recording was greater in cells dialyzed with these inhibitors. To quantify the effects of PMCA inhibitors on hair bundle fluorescence, we measured normalized fluorescence intensities before mechanical stimulation from line scan images. Each bundle was deflected for 100 msec and its fluorescence intensity was recorded, approximately once per minute. We plotted the fluorescence intensities against time after the onset of whole-cell recording and fit data collected during the first 400 sec of whole-cell recording with least-squared error lines (r^2 values, 0.8–1.0). For control cells the rate of fluorescence increase in hair bundles was 0.5 ± 0.2 units/sec (mean ± SD, n = 6). By contrast, fluorescence rose much faster in cells dialyzed with PMCA inhibitors. The rate for cells filled with vanadate was 2.2 ± 0.5 units/sec (n = 4); for cells filled with carboxyeosin the rate was 1.4 ± 0.4 units/sec (n = 3). The average rate for control cells was significantly lower than that for cells filled with vanadate (p = 0.003; one-tail Student's t test) or carboxyeosin (p = 0.03). We used an *in vitro* calibration to convert fluorescence units to the estimated free concentration of Ca^{2+} in hair bundles under these conditions (Fig. 7*A*). Approximately 200 sec after establishment of the whole-cell configuration, the average hair bundle Ca^{2+} concentration in control hair cells was 28 ± 7 nM (n = 4). By contrast, in cells filled with carboxyeosin, the concentration of Ca^{2+} had increased to 47 ± 3 nM (n = 3); in cells filled with vanadate, the concentration of Ca^{2+} had reached 255 ± 133 nM (n = 5). The average fluorescence intensities for the three groups at this time were 106 ± 22 units, 185 ± 10 units, and 654 ± 203 units, respectively.

To distinguish between a direct effect of inhibitors on bundle PMCA molecules and an increase in Ca^{2+} concentration resulting from inhibition of somatic PMCA (and SERCA) molecules, we compared the ratio of bundle fluorescence to somatic fluorescence in cells filled with carboxyeosin with the ratio in control cells (Fig. 7*B*). In two carboxyeosin-filled hair cells that failed to transduce, the ratio of bundle fluorescence to somatic fluorescence (0.45 ± 0.03, mean ± SE) was lower than that in three control cells (0.60 ± 0.05). In three carboxyeosin-filled cells that exhibited transduction currents, however, bundle fluorescence

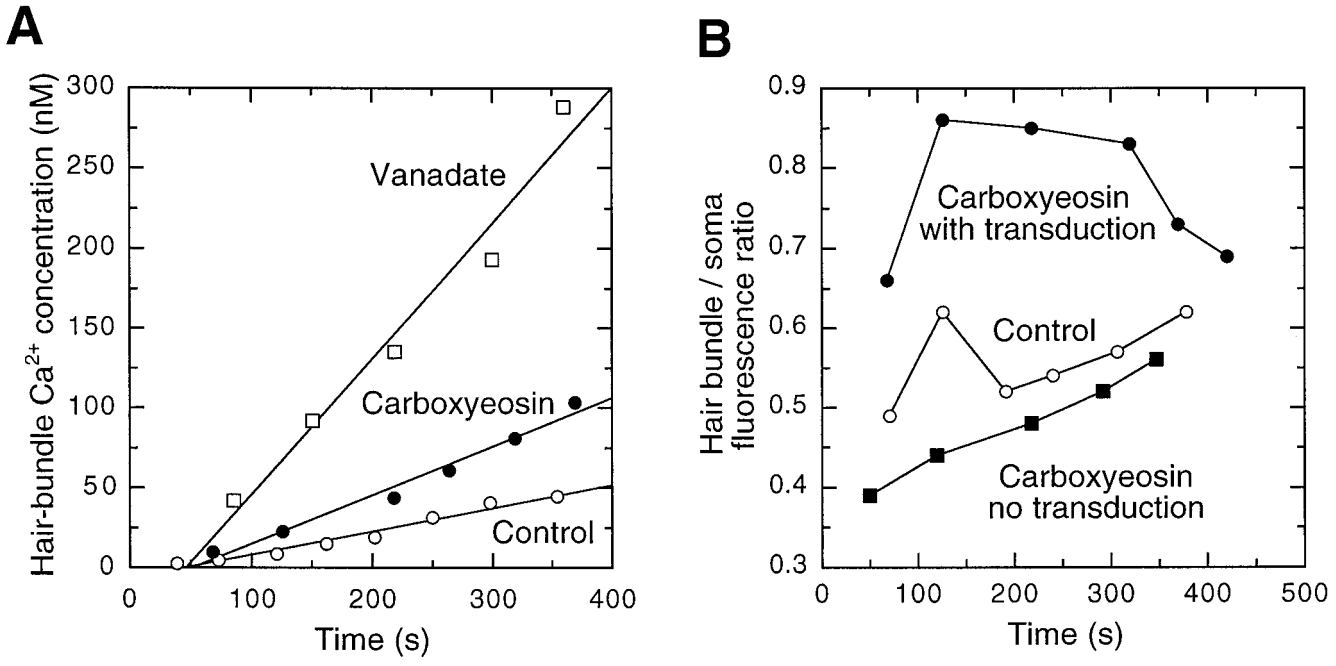

Figure 7. Quantitation of the fluo-3 fluorescence intensity of hair bundles filled with vanadate, carboxyeosin, and control solutions. *A*, The free calcium concentration of representative cells estimated with an *in vitro* calibration. To quantify the effects of PMCA inhibitors on hair bundle fluorescence, we measured fluorescence intensities before mechanical stimulation from line scan images. Ca^{2+} concentrations were plotted against time after the onset of whole-cell recording. Both the estimated Ca^{2+} concentration and the rate of concentration increase in the hair bundles of cells filled with vanadate or carboxyeosin exceeded those of control cells. For data collected during the first 400 sec of whole-cell recording, the plot of fluorescence intensity against time for each cell was fit with a minimal squared error line. *B*, Ratio of hair bundle fluorescence to somatic fluorescence in representative carboxyeosin cells with and without transduction and in a control cell with transduction. The fluorescence in hair bundles was highest relative to the somatic fluorescence when a PMCA inhibitor was present and substantial Ca^{2+} entry took place through transduction channels.

became relatively large when compared with somatic fluorescence (0.68 ± 0.02), indicating that this PMCA inhibitor affected the ability of hair bundles to remove Ca^{2+} that entered during transduction.

DISCUSSION

Present at high density in hair bundle plasma membranes, PMCA is poised to play a crucial role in regulation of the Ca^{2+} concentration of the hair bundle. Our immunoblotting and immunoprecipitation experiments show that 140 and 170 kDa forms of PMCA reside in bundles. Because these molecular masses correspond to those of the major calmodulin binding proteins of hair bundles (Walker et al., 1993) and because the 5F10 antibody immunoprecipitates calmodulin binding proteins of these sizes (see Fig. 2*C*), our data confirm that PMCA is the major calmodulin binding protein of stereocilia (Walker et al., 1993; Crouch and Schulte, 1995). Although PMCA2b is a reasonable candidate for the PMCA of stereocilia (Crouch and Schulte, 1996), isoform-selective antibodies will be required to establish the presence of this or other isoforms within the hair bundle.

To demonstrate that PMCA is active in hair bundles, we measured extracellular Ca^{2+} efflux from hair cells, using Ca^{2+}-selective self-referencing electrodes. Although the net flux of Ca^{2+} over the entire hair cell surface should have been zero, we were able to detect local Ca^{2+} efflux by using electrodes with tips of a few micrometers in diameter. These experiments demonstrated that hair cells locally extrude substantial quantities of Ca^{2+}; consistent with the participation of PMCA, vanadate microinjection reduced Ca^{2+} efflux. For most membrane regions that we investigated, we observed local efflux. Two factors contributed to this observation. First, PMCA, and thus the source of Ca^{2+} efflux, is distributed relatively uniformly over the hair cell membrane. Second, the points of Ca^{2+} entry into hair cells are focal: many basolateral Ca^{2+} channels are clustered at synaptic zones (Roberts et al., 1990; Issa and Hudspeth, 1994), and transduction channels are located only near stereociliary tips. Consistent with this explanation, when the probe was positioned near the top of the bundle, we observed substantial Ca^{2+} influx on positive bundle deflection, presumably because of Ca^{2+} entering open transduction channels.

When the probe was positioned close to the base of the hair bundle, the average Ca^{2+} flux approximated the Ca^{2+} transport rate of stereociliary membranes. Had all 2000 PMCA molecules in a square micrometer of membrane contributed equally, this flux would correspond to a pumping rate of 1.5 Ca^{2+} per PMCA per second. This value must, however, underestimate the actual efflux under these conditions. First, the method measured net flux; local efflux of Ca^{2+} from stereociliary membranes was counteracted by influx through nearby transduction channels. Furthermore, the electrode efficiency is not known accurately (Smith et al., 1994) and the probe was not juxtaposed perfectly to the stereociliary membrane. Most importantly, because the flux experiments used a low extracellular Ca^{2+} concentration (50 μM), Ca^{2+} entry into hair cells should have been greatly reduced when compared with the influx in the I_{TOC} experiments for which cells were exposed to 4 mM Ca^{2+}. The pumping rate during the flux measurements should have been far below the maximal turnover rate for the pump.

Additional evidence for active bundle PMCA molecules

stemmed from analysis of I_{TOC}, an outward current component elicited by mechanical stimuli. This current activated immediately and depended on the presence of extracellular Ca^{2+}. Although not conclusive, our pharmacological data support the hypothesis that I_{TOC} arose from electrogenic activity of PMCA. Assignment of I_{TOC} to PMCA activity would be strengthened if the PMCA inhibitor La^{3+} (Carafoli, 1991), applied extracellularly, could be used specifically to inhibit this current. Because La^{3+} eliminates transduction (Sand, 1975), however, the ion, unfortunately, should inhibit I_{TOC} regardless of the origin of the outward current.

If I_{TOC} can be attributed to PMCA activity, then the normalized amplitude of I_{TOC} can be used to estimate the turnover rate of bundle PMCA. In our preparation the number of intact tip links (Assad et al., 1991) and the number of functional transduction channels are such that a typical stereocilium probably contained only one functional 100 pS transduction channel (Crawford et al., 1991; Denk et al., 1995). Because the 80 mV driving force in our experiments should have produced a transduction current of −8 pA per stereocilium and because I_{TOC} averaged 0.04 pA per picoampere of inward transduction current (see Results), I_{TOC} of one stereocilium should have measured 0.3 pA. If one Ca^{2+} is exchanged for one H^+, the 3 amol of Ca^{2+} ions leaving a stereocilium per second would have been pumped by 2000 molecules of PMCA operating at a turnover number of 120/sec. If the pumps operated below their maximal rate or if our measurement underestimated I_{TOC}, then the maximal turnover rate would have been higher. Our value falls within the range estimated for PMCA in erythrocytes (50–300/sec; Garrahan, 1986; Rega, 1986). Taken together, our data are broadly consistent with ~2000 PMCA molecules per square micrometer of stereociliary membrane, each capable of operating at a maximal turnover rate exceeding 100/sec.

Contribution of PMCA to stereociliary Ca^{2+} regulation

Although the surface density of PMCA on the stereociliary membrane is similar to that inferred for PMCA on the basolateral surface of the hair cell (Tucker et al., 1996; Wu et al., 1996), PMCA should play a more important role in stereocilia than in the soma. Not only are stereocilia unable to sequester Ca^{2+} in intracellular organelles, but the cytoplasmic volume per PMCA molecule is much smaller in stereocilia than in the soma; an equivalent amount of Ca^{2+} therefore should be extruded from stereocilia more rapidly than from the soma.

Consistent with a critical role for PMCA in stereocilia, the PMCA inhibitors vanadate and carboxyeosin rapidly increased the concentration of Ca^{2+} in hair bundles. Inhibition of somatic Ca^{2+} pumps (Tucker and Fettiplace, 1995) and the subsequent rise in Ca^{2+} load faced by the bundle probably also contributed to the observed rise in bundle Ca^{2+} concentration. Nevertheless, the increase in bundle Ca^{2+} concentration in carboxyeosin-filled hair cells that had substantial transduction currents indicates that PMCA plays an active role in extruding Ca^{2+} entering during transduction. Indeed, bundle Ca^{2+} signals elicited by mechanical stimulation can be fit only with models that invoke a robust Ca^{2+} extrusion mechanism (E. A. Lumpkin and A. J. Hudspeth, unpublished observations). Until the Ca^{2+} binding properties and concentration of mobile Ca^{2+} buffers in stereocilia are determined, the contribution of PMCA to bundle Ca^{2+} regulation *in vivo* can be estimated only qualitatively. Nevertheless, our data indicate that PMCA is one of the dominant factors controlling the concentration of Ca^{2+} in stereocilia.

Consequences of high PMCA density

The measured PMCA activity has several significant implications. First, because PMCA is thought to exchange one H^+ for each Ca^{2+} transported (Hao et al., 1994), the hair bundle pH should drop precipitously during transduction unless stereocilia contain robust H^+ extrusion or buffering mechanisms. Indeed, electrogenic H^+ extrusion, outward in direction, could contribute to I_{TOC}. Second, because one ATP is consumed for every Ca^{2+} transported, hair bundle PMCA should impose a substantial energy load on a hair cell, as suggested for somatic Ca^{2+}-ATPases (Tucker et al., 1996); a 200 msec, 0.3 pA pump current in a single stereocilium would consume 1 mM ATP there. ATP consumption by hair bundle PMCA may well be among the dominant energy loads faced by a hair cell. Nevertheless, entry of Ca^{2+} through transduction channels must be sufficiently crucial to hair cell function that the cell can tolerate this energy expenditure.

Transcellular Ca^{2+} flux and extracellular Ca^{2+} gradients

Although saccular endolymph has a bulk Ca^{2+} concentration of ~260 μM (Corey and Hudspeth, 1983), PMCA may elevate substantially the extracellular concentration of Ca^{2+} close to the apical surfaces of hair cells. The amount of Ca^{2+} entering through basolateral channels should exceed that entering through transduction channels, and mobile Ca^{2+} buffers should distribute the ion throughout the cell. In a steady state, influx of Ca^{2+} is matched by efflux across the plasma membrane; the high density of hair bundle PMCA should permit bundles to extrude a fraction of this Ca^{2+} load, producing a transcellular Ca^{2+} flux from the basolateral to the apical surface. Transcellular Ca^{2+} flux is well established in renal epithelia, where calbindin shuttles Ca^{2+} from apical Ca^{2+} channels to basolateral Ca^{2+} pumps and transporters (Bronner, 1989; Friedman and Gesek, 1995).

Our calculations suggest that the concentration of Ca^{2+} near the saccular surface could be 200 μM greater than that of the bulk endolymph (see Appendix). Local Ca^{2+} conductances might reduce this value modestly, but diffusional obstructions such as the otolithic membrane and otoconia should increase it. Although the issue clearly requires further investigation, we speculate that PMCA molecules increase the concentration of Ca^{2+} surrounding hair bundles; a locally elevated extracellular Ca^{2+} concentration could speed adaptation (Eatock et al., 1987; Ricci and Fettiplace, 1997) and accentuate bundle twitches (Benser et al., 1996). In the mammalian cochlea, PMCA is elevated strikingly on hair bundles of mature outer hair cells and appears to be absent on their basolateral surfaces (Crouch and Schulte, 1995). With a bulk endolymphatic Ca^{2+} concentration of only 30 μM (Bosher and Warren, 1978), the consequences of high PMCA activity should be still more significant.

APPENDIX

Isolated cell model

We modeled a single hair bundle as a cylinder 6 μm tall and 4 μm in diameter. To simplify calculations, we positioned 66 point sources of Ca^{2+} along the surface of the cylinder, ~1 μm apart in each dimension, and divided the total Ca^{2+} efflux among these sources; each point source therefore represented the contribution of ~15,000 PMCA molecules. The basal activity of each PMCA molecule was assumed to be 1.5/sec; during stimulation this value increased linearly over 300 msec. Like isolated hair cells, only some of the stereocilia of the model bundle have active transduc-

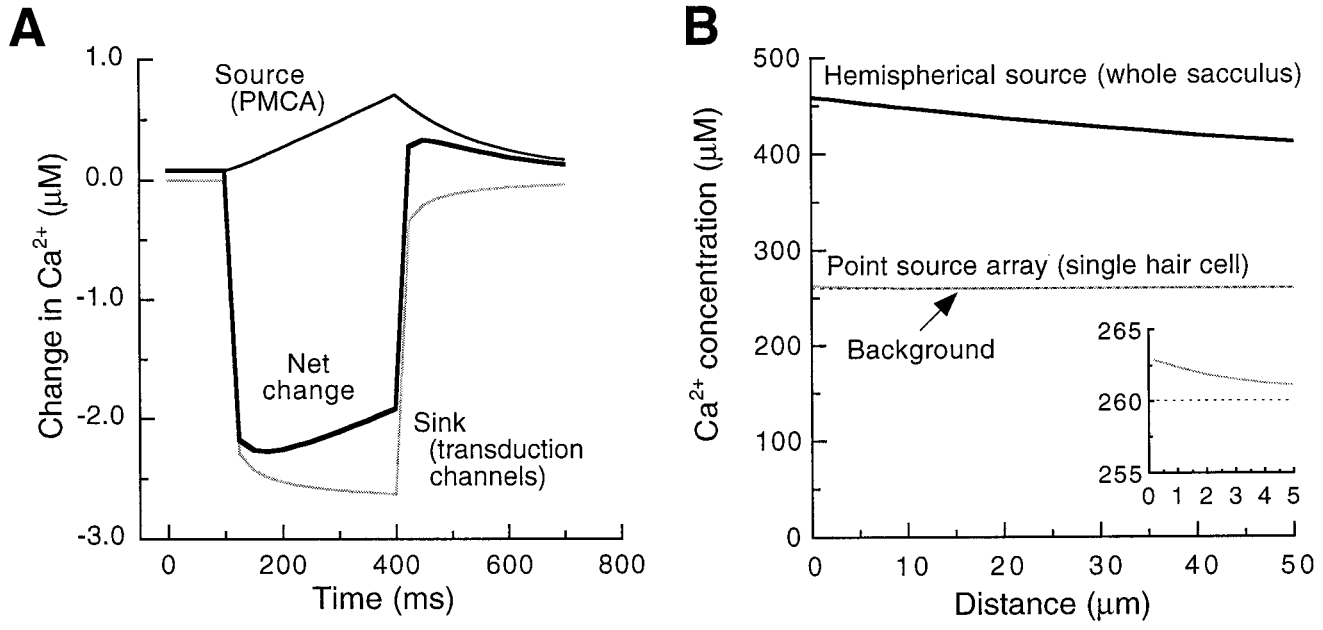

Figure 8. Modeling extracellular Ca^{2+} gradients. *A*, The concentration of Ca^{2+} 1 μm from the model hair bundle described in Appendix during mechanical stimulation. The contributions from Ca^{2+} pumps (*thin black line*) and transduction channels (*gray line*), as well their sum (*thick black line*), are plotted separately. *B*, The modeled gradients in Ca^{2+} concentration above the saccular apical surface (*black lines*) or above a single hair bundle (*gray line*). The concentration gradient for the model bundle is magnified in the *inset*. The background concentration of Ca^{2+} (260 μM) is indicated by the *dotted line*.

tion channels and hence display elevated pump turnover; average turnover during mechanical displacement therefore was increased to only 15/sec. After termination of the step, pump turnover was reduced exponentially to the resting value with a time constant of 150 msec. Because our transduction currents are typically smaller than −100 pA, our model incorporated seven point sinks (transduction channels), each with a maximum 8 pA transduction current, located atop the model cylinder. The fraction of current carried by Ca^{2+} was assumed to be 5% (Lumpkin et al., 1997). The measurement position was located 1 μm above the center of the top of the cylinder.

For a point source, extruding into a semi-infinite space a current i of a compound with valence z and diffusion coefficient D, the concentration C at radius r is (Berg, 1993):

$$C(r) = \frac{i}{4\pi zFDr}\, erfc\frac{r}{(4Dt)^{1/2}} \quad t < \infty.$$

The response to a sustained stimulus is:

$$C(r) = \frac{i}{4\pi zFDr} \quad t = \infty.$$

After a current step of finite time (t_0) is terminated, the concentration declines as:

$$C(r) = \frac{i}{4\pi zFDr}\left\{erfc\frac{r}{(4Dt)^{1/2}} - erfc\frac{r}{[4D(t-t_0)]^{1/2}}\right\} \quad t > t_0.$$

The simulation is plotted in Figure 8*A*; note that the drop in extracellular Ca^{2+} concentration that results from transduction channel opening develops rapidly and dominates the increase in extracellular Ca^{2+} as the ion enters the hair bundle and then is pumped out. All of these changes in Ca^{2+} are fast relative to the sampling rate of the Ca^{2+} electrode (<1 Hz).

Can this small drop in Ca^{2+} concentration during transduction be measured with Ca^{2+}-selective self-referencing electrodes? During a sustained mechanical displacement the Ca^{2+} concentration 1 μm from the model bundle should be ~2 μM lower than the background concentration of 50 μM. Given the properties of the Ca^{2+} measurement electrodes, we would expect the following signal (Smith et al., 1994):

$$\Delta V \approx \frac{S\, R_v(\Delta C/C_b)}{2.3}$$

$$\Delta V \approx \frac{(28\text{ mV})(0.45)(2\ \mu\text{M}/50\ \mu\text{M})}{2.3}$$

$$\Delta V \approx 240\ \mu\text{V}.$$

This value is comparable in amplitude to the response shown in Figure 3*C*.

Transcellular Ca^{2+} flux and extracellular Ca^{2+} gradients

The extracellular gradient in Ca^{2+} concentration above the apical surfaces of hair cells should depend on the net Ca^{2+} flux from basolateral to apical membranes, on the binding and diffusional properties of mobile Ca^{2+} buffers, and on the distribution of PMCA molecules. Because healthy cells have substantial resting transduction currents, their resting potentials lie at the more positive end of the measured range (−60 to −50 mV; Hudspeth and Lewis, 1988). Under these conditions the amount of Ca^{2+} entering through basolateral Ca^{2+} channels should exceed that entering through transduction channels (Lenzi and Roberts, 1994). For example, although run-down and cell isolation treatments diminish the total Ca^{2+} conductance, the basolateral Ca^{2+} current at −50 mV still exceeds −20 pA (Hudspeth and Lewis, 1988; E. Yamoah and P. Gillespie, unpublished data). For a hair cell *in situ*, the Ca^{2+} current may be substantially greater.

By contrast, an ensemble of transduction channels with maximal 200 pA current, 15% open at rest and admitting 5% of the current as Ca^{2+}, should produce an apical Ca^{2+} current of only −1.5 pA. Because the conductance of voltage-activated basolateral Ca^{2+} channels grows steeply with membrane depolarization, net basolateral Ca^{2+} influx should be even more pronounced during mechanical stimulation.

Hair cells have high concentrations of mobile Ca^{2+} buffers (Roberts, 1993; Tucker and Fettiplace, 1996). Because of their Ca^{2+} binding and diffusional properties, these buffers should distribute Ca^{2+} throughout the cell. The effect of the Ca^{2+} buffer is to enhance the apparent diffusion of Ca^{2+}; if the concentration of mobile buffer is substantially greater than the total cytosolic Ca^{2+} concentration, then the diffusion of Ca^{2+} is augmented by the ratio (Bronner, 1989):

$$A = \frac{D_B}{D_{Ca}} \cdot \frac{[B]}{K_D},$$

in which A is the augmentation of the diffusion of Ca^{2+}, D_B and D_{Ca} are the diffusion coefficients for the mobile buffer and for free Ca^{2+}, $[B]$ is the concentration of mobile buffer, and K_D is the dissociation constant for the Ca^{2+} buffer reaction. In the hair cell, where the mobile buffer has a behavior similar to that of 0.8 mM BAPTA (Roberts, 1993), diffusion may be enhanced 100-fold or more. The consequence is that an entering Ca^{2+} ion diffuses a very large distance before it is captured by a PMCA molecule. The hair bundle contains ~30% of the plasmalemma of a hair cell (Roberts et al., 1990); because the density of PMCA is at least as high on stereociliary membranes as on the somatic membrane (see Fig. 1), bundle PMCA molecules plausibly might extrude an equivalent fraction of the total resting Ca^{2+} influx.

To estimate the apical concentration gradient that might be produced by a transcellular Ca^{2+} flux, we considered the saccular epithelium to be a hemispherical source of Ca^{2+}, extruding the ion into a semi-infinite volume. More accurate representations of the source—for example a disk source, a collection of point sources corresponding to saccular bundles, or a collection of point sources corresponding to individual PMCA molecules—produce still greater local Ca^{2+} concentrations.

The time-dependent relation between concentration and distance for a hemispherical source is (Carslaw and Jaeger, 1959):

$$C = \frac{s}{4\pi D\, r\, r'}\left\{ 2(Dt/\pi)^{1/2}\left[e^{-(r-r')^2/4Dt} - e^{-(r+r')^2/4Dt}\right] - \left|r - r'\right| erfc\frac{|r-r'|}{2(Dt)^{1/2}} + (r+r')erfc\frac{r+r'}{2(Dt)^{1/2}}\right\},$$

in which s is the transport rate from the source, D is the diffusion coefficient, r is the distance from the center of the hemisphere, and r' is the radius of the hemisphere. At infinite time, this expression reduces to:

$$C = \frac{s}{2\pi D\, r}.$$

The Ca^{2+} current into a healthy hair cell at rest might measure −50 pA; over time, this influx of 260 amol of Ca^{2+} per second must be balanced by an equal extrusion via plasma membrane pumps and transporters. Of this input, we assumed that 30% is extruded by stereociliary PMCA (see above). Transport of 160 fmol of Ca^{2+} per second by the 2000 saccular hair bundles, coupled with the diffusion coefficient of Ca^{2+} (8×10^{-10} m^2/sec; Hille, 1992) and an approximate saccular radius of 160 μm (Jacobs and Hudspeth, 1990), suggests that the concentration of Ca^{2+} near the saccular surface could be 200 μM greater than that of the bulk endolymph (see Fig. 8*B*).

The additive effect of a large number of adjacent Ca^{2+} sources is striking; calculation for a single model hair bundle (see above) using the same values gives an elevated extracellular Ca^{2+} concentration of <5 μM at 1 μm (see Fig. 8*B* and *inset*). For the low Reynolds number at which hair bundles operate, stirring effects evoked by bundle vibration during natural stimuli should be negligible. During excitatory mechanical transduction Ca^{2+} entry through open transduction channels should reduce the extracellular Ca^{2+} concentration, but only by a few micromolar. As noted above, by greatly increasing basolateral Ca^{2+} entry, excitatory stimulation should *increase* the net transcellular Ca^{2+} flux, ultimately exaggerating the gradient.

REFERENCES

Adamo HP, Caride AJ, Penniston JT (1992) Use of expression mutants and monoclonal antibodies to map the erythrocyte Ca^{2+} pump. J Biol Chem 267:14244–14249.

Ammann D (1986) Ion-selective microelectrodes: principles, design and application. New York: Springer.

Assad JA, Corey DP (1992) An active motor model for adaptation by vertebrate hair cells. J Neurosci 12:3291–3309.

Assad JA, Shepherd GMG, Corey DP (1991) Tip-link integrity and mechanical transduction in vertebrate haircells. Neuron 7:985–994.

Benser ME, Issa NP, Hudspeth AJ (1993) Hair bundle stiffness dominates the elastic reactance to otolithic membrane shear. Hear Res 68:243–252.

Benser ME, Marquis RE, Hudspeth AJ (1996) Rapid, active hair bundle movements in hair cells from the bullfrog's sacculus. J Neurosci 16:5629–5643.

Berg HC (1993) Random walks in biology, Expanded Ed. Princeton, NJ: Princeton UP.

Bosher SK, Warren RL (1978) Very low calcium content of cochlear endolymph, an extracellular fluid. Nature 273:377–378.

Bronner F (1989) Renal calcium transport: mechanisms and regulation—an overview. Am J Physiol 26:F707–F711.

Burnham JA, Sterling CE (1984) Quantitative localization of Na-K pump sites in the frog sacculus. J Neurocytol 13:617–638.

Carafoli E (1991) Calcium pump of the plasma membrane. Physiol Rev 71:129–153.

Carslaw HS, Jaeger JC (1959) Conduction of heat in solids, 2nd Ed. Oxford: Oxford UP.

Corey DP, Hudspeth AJ (1979) Ionic basis of the receptor potential in a vertebrate hair cell. Nature 281:675–677.

Corey DP, Hudspeth AJ (1980) Mechanical stimulation and micromanipulation with piezoelectric bimorph elements. J Neurosci Methods 3:183–202.

Corey DP, Hudspeth AJ (1983) Kinetics of the receptor current in bullfrog saccular hair cells. J Neurosci 3:962–976.

Crawford AC, Evans MG, Fettiplace R (1991) The actions of calcium on the mechanoelectrical transducer current of the turtle hair cells. J Physiol (Lond) 434:369–398.

Crouch JJ, Schulte BA (1995) Expression of plasma membrane Ca-ATPase in the adult and developing gerbil cochlea. Hear Res 92:112–119.

Crouch JJ, Schulte BA (1996) Identification and cloning of site C splice variants of plasma membrane Ca-ATPase in the gerbil cochlea. Hear Res 101:55–61.

Denk W, Holt JR, Shepherd GMG, Corey DP (1995) Calcium imaging of single stereocilia in hair cells: localization of transduction channels at both ends of tip links. Neuron 15:1311–1321.

Eatock RA, Corey DP, Hudspeth AJ (1987) Adaptation of mechanoelectrical transduction in hair cells of the bullfrog's sacculus. J Neurosci 7:2821–2836.

Eberhard M, Erne P (1989) Kinetics of calcium binding to fluo-3 determined by stopped flow fluorescence. Biochem Biophys Res Commun 163:309–314.

Friedman PA, Gesek FA (1995) Cellular calcium transport in renal epithelia: measurement, mechanisms, and regulation. Physiol Rev 75:429–471.

Garrahan PJ (1986) Isolation and purification of the Ca^{2+} pump. I. The main difficulties and the first attempts. In: The Ca^{2+} pump of plasma membranes (Rega AF, ed), pp 45–65. Boca Raton, FL: CRC.

Gatto C, Milanick MA (1993) Inhibition of the red blood cell calcium pump by eosin and other fluorescein analogues. Am J Physiol 264:C1577–C1586.

Gillespie PG, Gillespie SKH (1997) Improved electrophoresis and transfer of picogram amounts of protein with hemoglobin. Anal Biochem 246:239–245.

Gillespie PG, Hudspeth AJ (1991a) High-purity isolation of bullfrog hair bundles and subcellular and topological localization of constituent proteins. J Cell Biol 112:625–640.

Gillespie PG, Hudspeth AJ (1991b) Chemiluminescence detection of proteins from single cells. Proc Natl Acad Sci USA 88:2563–2567.

Gillespie, PG, Hudspeth AJ (1993) Adenine nucleoside diphosphates block adaptation of mechanoelectrical transduction in hair cells. Proc Natl Acad Sci USA 90:2710–2714.

Goodno CC (1982) Myosin active-site trapping with vanadate ion. Methods Enzymol 85:116–123.

Gopalakrishna R, Anderson WB (1982) Ca^{2+}-induced hydrophobic site on calmodulin: application for purification of calmodulin by phenyl-Sepharose affinity chromatography. Biochem Biophys Res Commun 104:830–836.

Graf E, Verma AK, Gorski JP, Lopaschuk G, Niggli V, Zurini M, Carafoli E, Penniston JT (1982) Molecular properties of calcium-pumping ATPase from human erythrocytes. Biochemistry 21:4511–4516.

Hao L, Rigaud JL, Inesi G (1994) Ca^{2+}/H^{+} countertransport and electrogenicity in proteoliposomes containing erythrocyte plasma membrane Ca-ATPase and exogenous lipids. J Biol Chem 269:14268–14275.

Hasson T, Gillespie PG, MacDonald RB, Garcia J, Zhao YD, Yee AG, Mooseker MS, Corey DP (1997) Unconventional myosins in inner-ear sensory epithelia. J Cell Biol 137:1287–1307.

Hille B (1992) Ionic channels of excitable membranes. Sunderland, MA: Sinauer.

Hinds TR, Andreasen TJ (1981) Photochemical crosslinking of azidocalmodulin to the (Ca^{2+} Mg^{2+})ATPase at low Ca^{2+} concentrations. J Biol Chem 256:7877–7882.

Holton T, Hudspeth AJ (1986) The transduction channel of hair cells from the bull-frog characterized by noise analysis. J Physiol (Lond) 375:195–227.

Hudspeth AJ (1982) Extracellular current flow and the site of transduction by vertebrate hair cells. J Neurosci 2:1–10.

Hudspeth AJ (1989) How the ear's works work. Nature 341:397–404.

Hudspeth AJ, Lewis RS (1988) Kinetic analysis of voltage- and ion-dependent conductances in saccular hair cells of the bull-frog, *Rana catesbeiana*. J Physiol (Lond) 400:237–274.

Issa NP, Hudspeth AJ (1994) Clustering of Ca^{2+} channels and Ca^{2+}-activated K^{+} channels at fluorescently labeled presynaptic active zones of hair cells. Proc Natl Acad Sci USA 91:7578–7582.

Jacobs RA, Hudspeth AJ (1990) Ultrastructural correlates of mechanoelectrical transduction in hair cells of the bullfrog's internal ear. Cold Spring Harb Symp Quant Biol 55:547–561.

Jørgensen F, Kroese ABA (1995) Ca^{2+} selectivity of the transduction channels in the hair cells of the frog sacculus. Acta Physiol Scand 155:363–376.

Kao JP, Harootunian AT, Tsien RY (1989) Photochemically generated cytosolic calcium pulses and their detection by fluo-3. J Biol Chem 264:8179–8184.

Kosk-Kosicka D, Scaillet S, Inesi G (1986) The partial reactions in the catalytic cycle of the calcium-dependent adenosine triphosphatase purified from erythrocyte membranes. J Biol Chem 261:3333–3338.

Kuhtreiber WM, Jaffe LF (1990) Detection of extracellular calcium gradients with a calcium-specific vibrating electrode. J Cell Biol 110:1565–1573.

Läuger P (1991) Electrogenic ion pumps. Sunderland, MA: Sinauer.

Lenzi D, Roberts WM (1994) Calcium signaling in hair cells: multiple roles in a compact cell. Curr Opin Neurobiol 4:496–502.

Lumpkin EA, Hudspeth AJ (1995) Detection of Ca^{2+} entry through mechanosensitive channels localizes the site of mechanoelectrical transduction in hair cells. Proc Natl Acad Sci USA 92:10297–10301.

Lumpkin, EA, Marquis RE, Hudspeth AJ (1997) The selectivity of the hair cell's mechanoelectrical-transduction channel promotes Ca^{2+} flux at low Ca^{2+} concentrations. Proc Natl Acad Sci USA 94:10997–11002.

Macara IG (1990) Vanadium—an element in search of a role. Trends Biochem Sci 5:92–94.

Murphy AJ, Coll RJ (1993) Formation of a stable inactive complex of the sarcoplasmic reticulum calcium ATPase with magnesium, beryllium, and fluoride. J Biol Chem 268:23307–23310.

Myung J, Jencks WP (1994) Substrate specificity for catalysis of phosphoryl transfer by the calcium ATPase of sarcoplasmic reticulum. Arch Biochem Biophys 313:39–46.

Ohmori H (1985) Mechanoelectrical transduction currents in isolated vestibular hair cells of the chick. J Physiol (Lond) 359:189–217.

Pickles JO, Comis SD, Osborne MP (1984) Cross-links between stereocilia in the guinea pig organ of Corti, and their possible relation to sensory transduction. Hear Res 15:103–112.

Reeves JP (1991) Sodium–calcium exchange activity in plasma membrane vesicles. In: Cellular calcium. A practical approach (McCormack JG, Cobbold PH, eds), pp 283–298. Oxford: Oxford UP.

Rega AF (1986) From the discovery of the Ca^{2+} pump in plasma membrane to the demonstration of its ubiquitousness: a historical review. In: The Ca^{2+} pump of plasma membranes (Rega AF, ed), pp 45–65. Boca Raton, FL: CRC.

Ricci AJ, Fettiplace R (1997) Effects of calcium buffering and cyclic AMP on mechanoelectrical transduction in turtle auditory hair cells. J Physiol (Lond) 501:111–124.

Roberts WM (1993) Spatial calcium buffering in saccular hair cells. Nature 363:74–76.

Roberts WM, Jacobs RA, Hudspeth AJ (1990) Colocalization of ion channels involved in frequency selectivity and synaptic transmission at presynaptic active zones of hair cells. J Neurosci 10:3664–3684.

Sand O (1975) Effects of different ionic environments on the mechanosensitivity of the lateral line organs in the mudpuppy. J Comp Physiol [A] 102:27–42.

Smith PJS, Sanger RH, Jaffe LF (1994) The Ca^{2+} electrode: a new technique for detecting plasma membrane regions of Ca^{2+} influx and efflux. Methods Cell Biol 40:115–134.

Tucker T, Fettiplace R (1995) Confocal imaging of calcium microdomains and calcium extrusion in turtle hair cells. Neuron 15:1323–1335.

Tucker T, Fettiplace R (1996) Monitoring calcium in turtle hair cells with a calcium-activated potassium channel. J Physiol (Lond) 494:613–626.

Tucker T, Art JJ, Fettiplace R (1996) Routes of calcium entry and extrusion in turtle hair cells. Ann NY Acad Sci 781:123–137.

Walker RG, Hudspeth AJ (1996) Calmodulin controls adaptation of mechanoelectrical transduction by hair cells of the bullfrog's sacculus. Proc Natl Acad Sci USA 93:2203–2207.

Walker RG, Hudspeth AJ, Gillespie PG (1993) Calmodulin and calmodulin-binding proteins in hair bundles. Proc Natl Acad Sci USA 90:2807–2811.

Wu YC, Tucker T, Fettiplace R (1996) A theoretical study of calcium microdomains in turtle hair cells. Biophys J 71:2256–2275.

Yamoah EN, Gillespie PG (1996) Phosphate analogs block adaptation in hair cells by inhibiting adaptation-motor force production. Neuron 17:523–533.

Yamoah EN, Smith PJ (1994) Second messenger modulation of steady-state calcium efflux in *Aplysia* bag cells. Biol Bull 187:270.

Zhao YD, Yamoah EN, Gillespie PG (1996) Regeneration of broken tip links and restoration of mechanoelectrical transduction in hair cells. Proc Natl Acad Sci USA 93:15469–15474.